

A MULTI-TRANSITION HCN AND HCO⁺ STUDY OF 12 NEARBY ACTIVE GALAXIES: AGN VERSUS SB ENVIRONMENTS

M. KRIPS¹, R. NERI², S. GARCÍA-BURILLO³, S. MARTÍN¹, F. COMBES⁴, J. GRACIÁ-CARPIO³, AND A. ECKART⁵

Draft version October 31, 2018

ABSTRACT

Recent studies have indicated that the HCN-to-CO(J=1-0) and HCO⁺-to-HCN(J=1-0) ratios are significantly different between galaxies with AGN (active galactic nucleus) and SB (starburst) signatures. In order to study the molecular gas properties in active galaxies and search for differences between AGN and SB environments, we observed the HCN(J=1-0), (J=2-1), (J=3-2), HCO⁺(J=1-0) and HCO⁺(J=3-2) emission with the IRAM 30m in the centre of 12 nearby active galaxies which either exhibit nuclear SB and/or AGN signatures. Consistent with previous results, we find a significant difference of the HCN(J=2-1)-to-HCN(J=1-0), HCN(J=3-2)-to-HCN(J=1-0), HCO⁺(J=3-2)-to-HCO⁺(J=1-0) and HCO⁺-to-HCN intensity ratios between the sources dominated by an AGN and those with an additional or pure central SB: the HCN, HCO⁺ and HCO⁺-to-HCN intensity ratios tend to be higher in the galaxies of our sample with a central SB as opposed to the pure AGN cases which show rather low intensity ratios. Based on an LVG analysis of these data, i.e., assuming purely collisional excitation, the (average) molecular gas densities in the SB dominated sources of our sample seem to be systematically higher than in the AGN sources. The LVG analysis seems to further support systematically higher HCN and/or lower HCO⁺ abundances as well as similar or higher gas temperatures in AGN compared to the SB sources of our sample. Also, we find that the HCN-to-CO ratios decrease with increasing rotational number J for the AGN while they stay mostly constant for the SB sources.

Subject headings: galaxies: active — galaxies: ISM — radio lines: galaxies — galaxies: individual (NGC 1068, NGC 5194, NGC 4826, NGC 3627, NGC 4569, NGC 6951, NGC 6946, NGC 2140, M82, NGC6240, Mrk231, Arp220)

1. INTRODUCTION

Activity in galaxies can be attributed to two main phenomena, highly active star formation, also called starburst (SB), and mass accretion onto a supermassive black hole, often simply referred to as active galactic nucleus (AGN). Obviously, molecular gas plays not only a key role as fuel in the activity process but should also, in turn, be strongly affected by the activity. Depending on the type, degree and evolutionary phase of the activity, different physical processes can be involved in changing the excitation conditions and chemical layout of the molecular gas, whether it is through strong ultra-violet (UV) or X-ray radiation fields or kinematical processes such as galaxy interaction, large scale shocks, gas out- or inflow. Knowing the composition and characteristics of the molecular gas in active environments is thus essential for the understanding of the activity itself, its evolution and possible differences between AGN and SB activity. Because of the differences in the radiation fields accompanying AGN and SB activity, AGN are suspected to create excitation and chem-

ical conditions for the surrounding molecular gas significantly different from those in SB environments. Indeed, several recent studies, mainly based on molecular gas tracers such as CO, HCN, and HCO⁺(J=1-0), appear to support this hypothesis: the HCN-to-CO(J=1-0) intensity ratios appear to be significantly higher and the HCO⁺-to-HCN(J=1-0) intensity ratios significantly lower in AGN (e.g., NGC 1068, NGC 6951, M51) than in SB (e.g., M82, NGC 6946) environments (e.g., Sternberg et al. 1994, 1996; Kohno et al. 1999, 2001; Kohno 2003, 2005). The difference in the intensity ratios can have various origins such as a) systematically different gas densities, b) systematically different gas temperatures, c) different radiation fields (UV vs. X-rays) eventually yielding different HCN, HCO⁺ and/or CO abundances (e.g., Tielens & Hollenbach 1985; Blake et al. 1987; Sternberg & Dalgarno 1995; Lepp & Dalgarno 1996; Maloney et al. 1996), d) shocks, e) the evolutionary stage of the activity, particularly important for starburst, f) additional non-collisional excitation of the gas through IR pumping by UV/X-ray heated dust (e.g. García-Burillo et al. 2006; Weiß et al. 2007), and g) supernova explosions (SNe), especially important for the HCO⁺ excitation.

In each case, the thermal and chemical structures of the gas should significantly differ between SB and AGN dominated regions. We thus carried out IRAM 30m observations of three HCN and two HCO⁺ transitions in 12 nearby active galaxies (see Table 1) to study the excitation conditions in SB and AGN dominated regions and their differences mainly as function of their gas densities, temperatures and molecular abundances. The sources in

¹ Harvard-Smithsonian Center for Astrophysics, SMA project, 60 Garden Street, MS 78 Cambridge, MA 02138, USA, mkrips@cfa.harvard.edu, smartin@cfa.harvard.edu

² Institut de Radio Astronomie Millimétrique, Saint Martin d'Hères, F-38406, France; neri@iram.fr

³ Observatorio Astronómico Nacional (OAN) - Observatorio de Madrid, C/ Alfonso XII 3, 28014 Madrid, Spain; s.gburillo@oan.es, j.gracia@oan.es

⁴ Observatoire de Paris, LERMA, 61 Av. de l'Observatoire, 75014 Paris, France; Françoise.Combes@obspm.fr

⁵ Universität zu Köln, I.Physikalisches Institut, Zùlpicher Str. 77, 50937 Köln, Germany; eckart@ph1.uni-koeln.de

this sample have been selected according to the following criteria: 1.) presence of either SB and/or AGN activity; 2.) previously detected HCN($J=1-0$) emission; 3.) available information on the CO emission; 4.) a declination above -20° so that they are observable from the IRAM 30m telescope.

2. OBSERVATIONS

We observed HCN($J=1-0$), HCN($J=2-1$), HCN($J=3-2$), HCO^+ ($J=1-0$) and HCO^+ ($J=3-2$) in the centre ($<30''$) of 12 nearby active galaxies⁶ (Table 1, Fig. 1 and 2) with the IRAM 30m telescope at Pico Veleta (Spain) during January (HCN) and August 2006 (HCN+ HCO^+). In the January run, the AD set of SIS receivers was tuned in single side band mode to the redshifted frequencies of HCN($J=1-0$) at 3 mm, HCN($J=2-1$) at 2 mm and HCN($J=3-2$) at 1 mm. In the August run, the AD set of SIS receivers were tuned in single side band mode to the redshifted frequencies of HCO^+ ($J=1-0$) at 3 mm, HCN($J=2-1$) at 2 mm and HCN($J=3-2$) & HCO^+ ($J=3-2$) at 1 mm. We used the 1 MHz backends with an effective total bandwidth of 512 MHz at 3mm and the 4 MHz backends with an effective total bandwidth of 1024 MHz at 2 mm and 1 mm. We spent $\sim 1-4$ hours on each target resulting in line detections with good to excellent signal-to-noise ratios ($\text{SNRs} \geq 5$) for most of the sources. The atmospheric opacity at 225 GHz ranged between $\sim 0.1-0.2$ in $\sim 80\%$ of the time in January and between $\sim 0.2-0.3$ in August 2006. The (redshifted) HCN($J=2-1$) line is still far enough in frequency from the atmospheric water absorption line at 183.3 GHz to be detectable without any contamination. Unfortunately, the same water absorption line prevents a reliable observation of the HCO^+ ($J=2-1$) transition, which is ~ 1 GHz closer to the water line. Also, the 2 mm receiver performance in the 177.5-183 GHz window is severely reduced, yielding intolerably high system temperatures (>1500 K). We regularly checked the pointing on a nearby planet and/or bright quasar resulting in a pointing accuracy within a few arcseconds (i.e., $\sim 2-4''$).

3. DATA ANALYSIS

Throughout the paper, the temperature scale is equivalent to T_{mb} , i.e., main beam brightness temperature, which is defined as $T_{\text{mb}} = T_{\text{a}}^* F_{\text{eff}} / B_{\text{eff}}$. The beam ($\equiv B_{\text{eff}}$) and forward efficiencies ($\equiv F_{\text{eff}}$) together with the beam sizes are given in Table 2. As beam filling effects are a crucial point for the analysis of our data, especially since we are mainly interested in the intensity ratios between different line transitions, all derived intensity ratios have been very carefully corrected using beam filling factors (see also Table 3). We use the following definitions and relations:

$$R_{J_u, J_l/10}^{\text{mol}} = \frac{f_{J_u, J_l}^{-1} \cdot I_{J_u, J_l}^{\text{mol}}}{f_{10}^{-1} \cdot I_{10}^{\text{mol}}}, \quad J_u = 3, 2; \quad J_l = J_u - 1; \quad (1)$$

mol = HCN or HCO^+

with $R_{J_u, J_l/10}^{\text{mol}}$ being the line intensity ratio between the same molecule (i.e., HCN or HCO^+) at transition

($J=J_u \rightarrow J_l$) and transition ($J=1 \rightarrow 0$), $I_{J_u, J_l}^{\text{mol}}$ the intensity (see Equation 3) of the molecule at transition ($J=J_u \rightarrow J_l$) and f_{J_u, J_l} the filling factor (see Equation 4). The HCO^+ -to-HCN intensity ratio at transition ($J=J_u \rightarrow J_l$) is defined as:

$$R_{J_u, J_l}^{\text{HCO}^+/\text{HCN}} = \frac{I_{J_u, J_l}^{\text{HCO}^+}}{I_{J_u, J_l}^{\text{HCN}}}, \quad J_u = 3, 1; \quad J_l = J_u - 1; \quad (2)$$

$(f_{J_u, J_l}^{\text{HCN}} = f_{J_u, J_l}^{\text{HCO}^+})$

$I_{J_u, J_l}^{\text{mol}}$ is the intensity of the molecular line in K km s^{-1} at transition ($J=J_u \rightarrow J_l$) and defined as

$$I_{J_u, J_l}^{\text{mol}} = \int T_{\text{mb}}^{\text{mol}(J=J_u-J_l)} dv, \quad J_u = 3, 2, 1; \quad (3)$$

$J_l = J_u - 1;$
mol = HCN or HCO^+

f_{J_u, J_l} is the beam filling factor and defined as

$$f_{J_u, J_l} = \left(\frac{(\theta_s^{J_u, J_l})^2}{(\theta_s^{J_u, J_l})^2 + (\theta_b^{J_u, J_l})^2} \right)^a, \quad J_u = 3, 2, 1; \quad (4)$$

$J_l = J_u - 1$

with $\theta_s^{J_u, J_l} \equiv$ size of the HCN($J=J_u - J_l$) emission region (\simeq size of the HCO^+ ($J=J_u - J_l$) emission region), $\theta_b^{J_u, J_l} \equiv$ beamsize at the HCN($J=J_u - J_l$) ($\simeq \text{HCO}^+$ ($J=J_u - J_l$)) frequency (see Table 2); a is either 1 in case of a circular source or 0.5 in case of an elliptical source, i.e., one that fills the beam in one direction (in the elliptical case we thus assume the minor axis of the emission as estimate for θ_s to derive the beam filling factor while we use the Full Width at Half Maximum (FWHM) in the circular case).

Some of the more distant sources in our sample are significantly smaller ($\leq 5''$) than the beamsizes resulting in smaller filling factors than for the more nearby galaxies (see Table 3). The size of the HCN and HCO^+ emission region for each galaxy has been estimated from interferometric and/or single-dish HCN and/or HCO^+ maps where present or as a conservative upper limit from CO maps. Uncertainties of the order of 1-5'' in the assumed source sizes translate into a $\leq 20\%$ uncertainty in the intensity ratios. For most of the sources, we assume that the size of the HCN (HCO^+) emission region is similar in all three (two) transitions, i.e., $\theta_s^{10} \approx \theta_s^{21} \approx \theta_s^{32}$. However, if this assumption were invalid, i.e., the size of the emission in the higher transitions is actually smaller by up to a factor of 50% than in the ground state, the estimated filling factor ratios between the different transitions could be too high by up to a factor of 4. Thus, in the case of NGC 1068, we explicitly take into account that the HCN($J=3-2$), HCN($J=2-1$) and HCO^+ ($J=3-2$) emission are more compact (by a factor of ~ 1.5) than the HCN($J=1-0$) and HCO^+ ($J=1-0$) emission as indicated by recent SMA observation of the HCN($J=3-2$) and HCO^+ ($J=3-2$) emission in NGC 1068 (Krips et al. in prep.). As a conservative approach, we also use a lower size of the HCN($J=3-2$), HCN($J=2-1$) and HCO^+ ($J=3-2$) line emission for NGC 5194 whose interferometric maps also indicate a decreasing size of the emitting region with increasing rotational number (Table 3 Matsushita et al. 2005). If we did not account for these differences in source sizes at different transitions, we might underestimate the line ratios for the AGN

⁶ The HCO^+ emission from the three ULIRGs in our sample, namely Arp 220, Mrk 231 and NGC 6240, were taken from Graciá-Carpio et al. (2006).

sources. Consequently, the so determined intensity ratios can be regarded as conservative upper limits for these two cases.

As we observed a large on the fly map ($\sim 2'$) for M82 in HCN and HCO^+ , we were able to average the emission in all line transitions over the same region resulting in identical filling factors. We thus assume a filling factor of 1 for M82.

4. RESULTS

4.1. The sample

We detect all twelve galaxies in HCN($J=1-0$) and $\text{HCO}^+(J=1-0)$, eleven in HCN($J=2-1$), ten in HCN($J=3-2$), and seven in $\text{HCO}^+(J=3-2)$ (Table 3, Fig. 1 & 2). The HCN intensity ratios are listed in Table 4 and plotted in Fig. 3-5.

The diagrams (Fig. 3-5) clearly indicate significant differences in the intensity ratios between the different activity types in our sample (see also discussion in the next sub-Sections):

- 1.) $R_{J_u, J_l}^{\text{HCN}}$ is *low* (i.e., $\lesssim 0.4$) in the 'pure' AGN sources of our sample and *high* in those with a dominant SB (i.e., ≥ 0.4), suggesting an increasing $R_{J_u, J_l}^{\text{HCN}}$ with an increasing SB contribution. The most extreme examples of $R_{J_u, J_l}^{\text{HCN}}$ are: NGC 1068 (*low* $R_{J_u, J_l}^{\text{HCN}}$; AGN), NGC 6951 & Arp220 & NGC 6946 (*moderate* $R_{J_u, J_l}^{\text{HCN}}$; AGN+SB), and M82 (*high* $R_{J_u, J_l}^{\text{HCN}}$; SB).
- 2.) $R_{32/10}^{\text{HCO}^+}$ is *low* in the 'pure' AGN sources (i.e., ≤ 0.3) but also in the composite (AGN+SB) sources, while it is *high* for the 'pure' SB sources (i.e., > 0.4). In combination with $R_{32/10}^{\text{HCN}}$, this creates so three different regions, separating the composite sources from the 'pure' SBs and AGN. The most extreme examples for each group are: NGC 1068 (*low* $R_{32/10}^{\text{HCO}^+}$ & $R_{32/10}^{\text{HCN}}$; AGN), Arp 220 & NGC 6951 (*moderate* $R_{32/10}^{\text{HCO}^+}$ & *low* $R_{32/10}^{\text{HCN}}$; AGN+SB), and M82 (*high* $R_{32/10}^{\text{HCO}^+}$ & $R_{32/10}^{\text{HCN}}$; SB).
- 3.) $R_{J_u, J_l}^{\text{HCO}^+/\text{HCN}}$ is *low to moderate* in the 'pure' AGN and almost all composite sources (i.e., < 1), while it is *moderate to high* for the 'pure' starbursts (i.e., ≥ 1). The most extreme examples are: NGC 1068 (*low* $R_{J_u, J_l}^{\text{HCO}^+/\text{HCN}}$; AGN), Arp220 (*low* $R_{J_u, J_l}^{\text{HCO}^+/\text{HCN}}$; AGN+SB), NGC 6240 (*high* $R_{J_u, J_l}^{\text{HCO}^+/\text{HCN}}$; AGN+SB), NGC 6946 & M82 (*high* $R_{J_u, J_l}^{\text{HCO}^+/\text{HCN}}$; SB).

The apparent grouping of the two dominant activity types in our sample into different intensity ratios supports fundamental differences between the excitation conditions of the two main activity types. It seems highly unlikely that biases in filling factors could lead to such a systematic trend.

A comparison to CO data taken either from the literature or from previous IRAM 30m observations reveals no similar separation effect in the CO line transition ratios

for our sample (see Table 4). However, as a very interesting result, the HCN-to-CO luminosity ratios appear to decrease with increasing rotational number J in the AGN sources (Table 5), while those of the SB sources remain more or less constant or even slightly increase.

4.2. Individual sources

In this Section, we will discuss some individual sources of our sample, each representing a good example of one of the ratio-extremes described in the previous Section.

4.2.1. M82 - SB dominated galaxy

M82 is the best testcase for a "pure" (evolved) SB in our sample. We mapped the entire central disk in M82 with the IRAM 30m at 3 mm and obtained a number of discrete pointings along the disk at 2 mm and 1 mm. The HCN and HCO^+ data are in good agreement with previous measurements (e.g., Nguyen et al. 1992). The gas disk in M82 is known to house two giant PDRs (e.g., García-Burillo et al. 2002), probably also a central massive black hole in formation (e.g., Matsushita et al. 2000; Patruno et al. 2006) and a superbubble emerging from a past SNe (e.g. Weiß et al. 1999; Kronberg et al. 1981). A different gas chemistry could hence be at play in the centre than in the two PDRs. Thus, the HCN and HCO^+ intensity ratios, discussed here, have been averaged over the entire map, and taken at the eastern PDR position and at the centre to allow for a better comparison. The 30m observations indicate some variations especially of $R_{21/10}^{\text{HCN}}$, $R_{32/10}^{\text{HCN}}$ and $R_{32/10}^{\text{HCO}^+}$ between the position of the PDR and the nucleus (see Table 4), while $R_{J_u, J_l}^{\text{HCO}^+/\text{HCN}}$ seems to be quite similar between the PDR and the center. The averaged ratios are very similar to the PDR ones indicating that PDR chemistry may dominate the overall emission in the disk. The PDR position in M82 shows the highest $R_{J_u, J_l}^{\text{HCN}}$, $R_{32/10}^{\text{HCO}^+}$ and $R_{J_u, J_l}^{\text{HCO}^+/\text{HCN}}$ of all the sources in our sample (see filled red box in Fig. 3-5). The center in M82, however, seems to be, overall, similar to the other SB sources of our sample for most line ratios (compare next sub-Sections).

4.2.2. NGC 6946 - SB dominated galaxy

NGC 6946 is a local galaxy whose starburst activity is assumed to be much younger than that in M82. NGC 6946 is not part of a galaxy-merger or -interaction, as it is the case for M82 (e.g., Pisano & Wilcots 2000). No signs of any significant PDR have yet been found in this galaxy and also large-scale, high-velocity shocks do not seem to play a major role yet (e.g., Schinnerer et al. 2007). This difference to M82 in its SB properties may explain its location in the diagrams (Fig. 3-5) with respect to M82, i.e., in the middle of the diagram, representing thus eventually a different type of starburst activity. As such, it might set tight constraints to our comparison between AGN and SB and underline the importance of the evolutionary stage of the starburst.

4.2.3. NGC 1068 - AGN dominated galaxy

NGC 1068 is the best example in our sample for housing a pure AGN in a central radius of 1 kpc ($\equiv 14''$)⁷.

⁷ Please note, that ~ 10 - 20% of the overall HCN emission in NGC 1068 is located in the spiral arms (Tacconi et al. 1994) which

No strong evidence for any significant *nuclear* starburst has been reported so far (e.g., MIR: Laurent et al. 2000; NIR(PAH): Imanishi 2002; Optical/Near-UV: Cid-Fernandes et al. 2001). Marco & Brooks (2003) estimate that a compact nuclear starburst would contribute less than 1% to the total IR luminosity. Thus, NGC 1068 represents the best counter-part to M82 in terms of activity type. NGC 1068 appears to be always located in the opposite part of the diagrams in Fig. 3-5 with respect to M82, supporting the differences in the excitation conditions of the molecular gas suspected between AGN and SB environments. Moreover, Usero et al. (2004) have discussed the possibility of NGC 1068 harbouring a giant XDR in its nucleus that is used to explain the surprisingly high HCN-to-CO and low HCO⁺-to-HCN luminosity ratios (see also Table 5). The potential prototypical XDR nature of the AGN in NGC 1068 classifies this source as an ideal counter-part to the PDR-dominated galaxy M82, in terms of effects of the radiation field onto the surrounding gas chemistry.

4.2.4. NGC 5194 - AGN dominated galaxy

Besides NGC 1068, the centre in NGC 5194 is most likely dominated by an AGN as well. This source is assumed to be in a post SB stage in which the massive star formation has already disappeared (e.g., Thronson et al. 1991; Sauvage et al. 1996; Greenawalt et al. 1998); its nuclear activity is assumed to be caused by a low-luminosity active galactic nucleus of LINER type (e.g., Ho, Filippenko, & Sargent 1997). NGC 5194 is located close to NGC 1068 in all diagrams (Fig. 3-5), substantiating the differences between AGN and SBs in our sample. It is also one of the few sources for which a high HCN-to-CO but low HCO⁺-to-HCN(J=1-0)⁺ intensity ratio has been found (see Table 5).

4.2.5. NGC 6951 - AGN+SB galaxy

The best example of a composite source in our sample likely is NGC 6951 (highlighted with a filled green triangle in Fig. 3-5). It is known to house a prominent SB ring (e.g., optical: Márquez & Moles 1993; Wozniak et al. 1995; Rozas, Beckman, & Knapen 1996; González-Delgado et al. 1997; radio: Vila et al. 1990; Saikia et al. 1994) as well as a Seyfert type 2/LINER nucleus in its central 20'' (e.g., Boer & Schulz 1993; Ho, Filippenko, & Sargent 1997). Kohno et al. (1999) have mapped this source in HCN(J=1-0) with the Nobeyama array revealing that most of the HCN emission is concentrated in the SB ring, similar to the CO emission. Probably due to missing sensitivity and angular resolution ($\sim 3-4''$), they fail to detect HCN(J=1-0) emission in the very centre (inner 2''). However, recent high angular resolution observations of HCN(J=1-0) in NGC 6951 carried out in the extended configuration of the IRAM PdBI show compact HCN emission in the centre as well (Krips et al. 2007) indicating a high HCN-to-CO(J=1-0) luminosity ratio of ~ 1 . The interferometric maps suggest that the HCN emission in the SB ring

are possibly dominated by star formation. However, even for the largest beam-size of 29'' the spiral arms should only marginally ($\sim 10\%$) contribute to the detected HCN emission in the 30m beam. The same is true for HCO⁺.

dominates the lines measured with the IRAM 30m telescope while the central HCN (and HCO⁺) emission probably contributes only marginally (less than 10%) to the observed brightness temperatures with the IRAM 30m. This explains the location of NGC 6951 in Fig. 3, close to the SB dominated sources in our sample. It has to be mentioned, though, that we might miss part (i.e., $\sim 30-40\%$) of the HCN(J=3-2) and HCO⁺(J=3-2) emission from the SB ring because of the lower beam size at these frequencies as recent SMA observation of the HCN(J=3-2) emission in NGC 6951 indicate (Krips et al., in prep.). However, this only slightly changes the position of NGC 6951 in Fig. 3-5. The HCO⁺ emission separates it significantly from the evolved starburst M82, similar to NGC 6240 and Arp 220. This may be either a consequence of the evolutionary stage of the starburst or the additional existence of an AGN.

4.2.6. Arp 220 - ULIRG (1 AGN + 1 SB nucleus)

Arp 220 is the prototypical ULIRG and as such represents well the higher-activity ULIRG population in our sample. A SB is outweighing the centre of Arp220 (e.g., Risaliti et al. 2006, and references therein) but an AGN may be present in at least one of the two nuclei though this is still controversial (e.g., Sanders 1988; Haas et al. 2001; Imanishi et al. 2006; Downes & Eckart 2007). The central (i.e., 2-4'') molecular gas emission in Arp 220 is concentrated in two peaks, very similar thus in its gas morphology to NGC 1068. Despite the differences in origin for the gas morphology of these two galaxies, i.e., two nuclei in Arp 220 (e.g., Sakamoto et al. 1999) versus a (probably) warped disk in NGC 1068 (e.g., Schinnerer et al. 2000), the beam filling factor ratios in the 30m beam should be very similar for the two sources (when assuming similar source sizes in all transitions), making the differences between their spectra even more pronounced, especially in the HCN transitions (Fig. 1). Even if we account for smaller source sizes for the higher transitions in NGC 1068 (which actually leads to different filling factors between NGC 1068 and Arp 220; see Table 3), $R_{J_u, J_l/10}^{\text{HCN}}$ is still significantly lower in NGC 1068 than in Arp 220. Interestingly, the situation for $R_{32/10}^{\text{HCO}^+}$ and $R_{J_u, J_l}^{\text{HCO}^+/\text{HCN}}$ is much different: here the ratios of both sources are very similar to each other. This potentially differentiates Arp 220 significantly from M82 and the composite sources and, together with NGC 6240 (see next sub-Section), may indicate that the ULIRGs have to be eventually handled as a different 'class' in our sample, i.e., separate from the local starbursts and composite sources. Also, Arp 220 is located close to NGC 6946 in the $R_{J_u, J_l/10}^{\text{HCN}}$ diagram (Fig. 3) but farther away from it in those including HCO⁺. Its intensity ratios seem to be more like those of NGC 6951, which has a dominating starburst but also a central weak AGN (see previous Section). Aalto et al. (2007) recently discussed the possibility of an XDR changing the molecular gas chemistry as an alternative to IR pumping to explain the high HCN-to-HCN(J=3-2) intensity ratios detected in Arp 220 by them.

4.2.7. NGC 6240 - ULIRG (2 AGN)

The two nuclei in NGC 6240 have been recently found to *both* harbor an AGN in addition to the very pronounced SB in this evolved merger (e.g., Komossa et al. 2003). Most of the molecular gas as well as dust appears to be located between the two nuclei (e.g., Bryant & Scoville 1999; Tacconi et al. 1999; Nakanishi et al. 2005; Iono et al. 2007) as opposed to Arp220 in which two gas disks may still be present (e.g., Sakamoto et al. 1999). Iono et al. (2007) also find evidence for a gas outflow/inflow that either is connected to starburst superwinds or outflows from the AGN. The existence of these and the two AGN in NGC 6240 may create exceptional and very extreme conditions for the molecular gas in the central region of NGC 6240. Similar to Arp 220, it is located close to NGC 6946 in the HCN diagram but closer to NGC 6951 in the diagram displaying $R_{32/10}^{\text{HCO}^+}$ (Fig. 4). However, in the $R_{J_u, J_l}^{\text{HCO}^+/\text{HCN}}$ diagram (Fig. 5), it seems to populate a very own region, quite separate from the rest, which may be linked to the extreme conditions in its centre.

5. LVG SIMULATIONS

We have run simulations of the excitation conditions for HCN and HCO^+ using the Large Velocity Gradient (LVG) approximation in MIRIAD to connect the observed intensity ratios with physical parameters such as kinetic gas temperature, gas density and molecular abundances. Although we find differences in the values obtained for HCO^+ between the LVG code used in MIRIAD and RADEX, we have concentrated our analysis on the MIRIAD code. The differences between the two codes seem to be only present for gas regions with very high HCO^+ column densities ($\gg 10^{15} \text{cm}^{-2} \text{km}^{-1} \text{s}$) that lie, however outside the range studied in this paper. For lower column densities, RADEX and the LVG code in MIRIAD produce almost identical results. We think that the difference could be either a consequence of a different 'parameter sampling' between the codes or different assumptions that start to fail for higher column densities in one of the two codes.

We assume a one component model for the LVG analysis, i.e., all HCN as well as HCO^+ transitions originate from the same region underlying the same gas temperature and density. We carried out a reduced χ^2 -test to constrain the above mentioned parameters; the χ^2 -test includes constraints based on $R_{J_u, J_l}^{\text{HCN}}$, $R_{10/10}^{\text{HCO}^+/\text{HCN}}$ and $R_{32/10}^{\text{HCO}^+}$ (Table 4).

We chose 4 exemplary sources in our sample, each representing one of the activity types and one of the ratio-groups: NGC 1068 as example of a pure AGN, NGC 6951 as example of a composite source, M82 as example of a pure SB, and NGC 6240 as the example with the most extreme intensity ratios among the three ULIRGs in our sample. For the LVG analysis, we varied the gas temperature in a range of $T_k=20\text{-}240$ K using steps of 20 K, the H_2 volume densities in a range of $n(\text{H}_2)=10^{1..7} \text{cm}^{-3}$, the $\text{HCN}(J=1-0)$ column densities per velocity interval in a range of $N(\text{HCN}(J=1-0))/dv \simeq 10^{11..19} \text{cm}^{-2} \text{km}^{-1} \text{s}$ and the HCO^+ -to-HCN abundance ratios in a range of $[\text{HCN}]/[\text{HCO}^+]=0.01\text{-}50$. We also base the discussion and simulations on the following definitions and rela-

tions:

$$Z(\text{HCN}) \equiv [\text{HCN}]/[\text{H}_2] \equiv n(\text{HCN})/n(\text{H}_2) \quad (5)$$

with $Z(\text{HCN})$ being the fractional abundance of HCN, $[\text{X}]$ the molecular abundance of the molecule X and $n(\text{X})$ the volume density of X in units of cm^{-3} . We then have

$$N(\text{HCN})/dv = Z(\text{HCN})/(dv/dr) \times n(\text{H}_2); \quad (6)$$

with $N(\text{HCN}) = n(\text{HCN}) \times dr$

where $N(\text{HCN})/dv$ is the HCN column density per velocity interval in units of $\text{cm}^{-2}/(\text{km s}^{-1})$, and dv/dr the "velocity gradient" in units of $\text{km s}^{-1}/\text{pc}$.

Fig. 6 & 7 and Table 6 show the results of the LVG analysis with the lowest χ^2 -values. Please note that we find two solutions respectively with similarly low χ^2 -values for NGC 1068 and NGC 6951. The contours in the plots encircle regions with $\chi^2 \leq 1$ and are color-coded following the previous Figures (NGC 1068: blue; NGC 6951: green; M82: red; NGC 6240: yellow). The HCN abundance is additionally indicated in grey lines decreasing in thickness from $10^{-5}(\text{km s}^{-1}/\text{pc}^2)^{-1}$ to $10^{-9}(\text{km s}^{-1}/\text{pc}^2)^{-1}$ in logarithmic steps of 1 based on equation 7. The standard (galactic) value for the HCN abundance found in galactic clouds is $Z^s(\text{HCN})=2 \times 10^{-8}$. Giving a velocity range of $\sim 100\text{-}500 \text{km s}^{-1}$ (compare Table 3) for this sample and assuming typical sizes of $\sim 100\text{-}500 \text{pc}$, we can constrain dv/dr to be in the range of $\sim 0.2\text{-}5 \text{km s}^{-1}/\text{pc}$. This results in a range of $Z^a(\text{HCN})/(dv/dr) \simeq 10^{-9}\text{-}10^{-7} (\text{km s}^{-1}/\text{pc}^2)^{-1}$ if assuming standard HCN abundances. However, for the AGN sources in our sample dv/dr is probably rather $\sim 1\text{-}5$ (large velocity width ($\sim 300 \text{km s}^{-1}$) and quite compact gas regions ($\leq 100 \text{pc}$) as opposed to $\sim 0.2\text{-}1$ for the (local) SB(+AGN) dominated sources (covering a more extended region of a few 100 pc than the AGN; e.g., M82 or NGC 6951), i.e.,

$$Z^s(\text{HCN})/(dv/dr)_{\text{AGN}} \lesssim 2 \times 10^{-8} (\text{km s}^{-1} \text{pc}^2)^{-1} \quad (7)$$

while

$$Z^s(\text{HCN})/(dv/dr)_{\text{SB}} \gtrsim 2 \times 10^{-8} (\text{km s}^{-1} \text{pc}^2)^{-1} \quad (8)$$

if taking a standard $Z^s(\text{HCN})$.

The LVG analysis most strikingly constrains the molecular gas densities in the AGN and SB(+AGN) sources. While HCN and HCO^+ emission in the SB dominated sources, such as M82 and NGC 6951, seem to emerge from regions with high H_2 densities in the range of $n(\text{H}_2)=(10^4\text{-}10^{6.5}) \text{cm}^{-3}$, the HCN and HCO^+ emission in sources of our sample with a pure AGN seem to be restricted to regions with gas densities of $n(\text{H}_2) \leq 10^{4.5} \text{cm}^{-3}$. The LVG analysis also restricts the kinetic gas temperatures to be below <120 K for the SB sources while the pure AGN cases appear to have no upper limit for T_k . The possibility of significantly higher temperatures in AGN has been already discussed for NGC 5194 by Matsushita et al. (1998) to explain the ^{13}CO emission in this source. A high kinetic temperature of $T_k > 70$ K has been also reported for NGC 1068 before by Sternberg et al. (1994). We furthermore find tendentially larger HCN abundances in the AGN sources than in the SB sources which may even lie significantly

above $Z^s(\text{HCN})$ by a factor of ~ 2 -200. M82 thereby seems to denote a different extreme, i.e., having an HCN abundance that appears to be lower by at least an order of magnitude than $Z^s(\text{HCN})$. We also find an extremely low $[\text{HCN}]/[\text{HCO}^+]$ abundance ratio of ≤ 1 that implies a very low HCN abundance and/or an additionally increased HCO^+ abundance. The $[\text{HCN}]/[\text{HCO}^+]$ abundance ratios seem to be around 10 (or more conservatively: $1 < [\text{HCN}]/[\text{HCO}^+] \leq 50$) for the rest.

The LVG analysis does not yield a very good solution for the HCO^+ emission in NGC 6240, which seems to stand out a little bit with its intensity ratios, especially in $R_{10/10}^{\text{HCO}^+/\text{HCN}}$, compared to the other two ULIRGs. The intensity ratios in Arp 220 and Mrk 231 are more like NGC 6951 in their ratios. This might indicate that a one-component model may be too simplistic in this case, while it reproduces well the values of the rest of the sample. Greve et al. (2006) present a two-phase LVG model for NGC 6240 (and Arp 220) that seems to fit nicely their data including also several transition of HCN and HCO^+ . However, our results on the gas densities and temperatures are not inconsistent with their findings, although our $n(\text{H}_2)$ seems a little bit lower than theirs; this may be though a consequence of our one-component model as their two phase model assumes a very dense plus a moderately dense gas phase which should result in an averaged and thus lower density in a one-phase model.

The systematically increased HCN abundance in the AGN sources of our sample implies that a mass determination through HCN in AGN may significantly overestimate the dense molecular gas mass (compare also Krips et al. 2007) when using the same conversion factor as for SBs/ULIRGs. Based on the LVG analysis and adopting HCN abundances in the range of $Z(\text{HCN})/(dv/dr) \approx (0.1-10) \times 10^{-7} \text{ pc}/(\text{km s}^{-1})$ with $T_k=40-240 \text{ K}$ for AGN, we find brightness temperatures (T_b) in the range of ~ 10 -100 K and H_2 gas densities of $n(\text{H}_2)=10^{2.0-10^{4.5}} \text{ cm}^{-3}$. Taking the molecular mass ($M_{\text{H}_2}[M_\odot]$) to HCN luminosity ratio ($L_{\text{HCN}}[(\text{K km s}^{-1} \text{ pc}^2)]$) of (e.g., Solomon, Downes & Radford 1992; Solomon, Radford & Downes 1990):

$$X(\text{HCN}) \equiv M_{\text{H}_2}/L_{\text{HCN}} = 2.1 \times n(\text{H}_2)^{0.5}/T_b, \quad (9)$$

we obtain $X(\text{HCN})=10_{-7}^{+10} M_\odot (\text{K km s}^{-1} \text{ pc}^2)^{-1}$ for the AGN sources. This conversion factor is ~ 2 times smaller than that derived for ULIRGs by Solomon, Downes & Radford (1992) and Greve et al. (2007) of $X(\text{HCN})=20_{-10}^{+30} M_\odot (\text{K km s}^{-1} \text{ pc}^2)^{-1}$ but agrees with that favored by Gao & Solomon (2004a) for their sample of nearby active galaxies and ULIRGs. An estimate of $X(\text{HCN})$ for the SB dominated sources in our sample yields a similar value to that of Solomon, Downes & Radford (1992) and Greve et al. (2007).

By comparing the brightness temperatures with the obtained kinetic temperatures (for the $J=1-0$ lines), we can give a very crude estimate of the optical depth τ , assuming $\tau = -\ln(1 - T_b/T_k)$. This yields $\tau \approx 0.4-1.0$ for the SB dominated sources, $\tau \approx 0.3-1.4$ for the AGN sources, $\tau \approx 0.3-1.8$ for the composite sources and $\tau \approx 0.7-1.0$ for NGC6240, indicating similar opacity ranges.

However, the ratio between T_b and T_k could be easily biased if the emission is very clumpy, artificially lowering the T_b/T_k ratio. As we probably average over many giant molecular cloud complexes, a clumpy structure may be indeed suspected in both SB galaxies (e.g., Zhang et al. 2001; Alonso-Herrero et al. 2002; Wilson et al. 2003; Galliano et al. 2005) and also for the gas/dust emission around AGN.

6. DISCUSSION

6.1. Chemical layout and excitation conditions

We briefly described various physical processes in the Introduction that can lead to the observed differences in the line and transition ratios between AGN and SB dominated galaxies. As first scenario, we mentioned gas densities and temperature effects (cases (a) and (b) in the Introduction): higher gas densities and/or temperatures tend to increase populations of higher-J CO levels and may lead, for a given column density, to a reduced $\text{CO}(J=1-0)$ line intensity (assuming that the gas densities are not that high to have a similar effect on the HCN emission). Given the *high* HCN-to- $\text{CO}(J=1-0)$ intensity ratios in AGN, this would consequently mean that the gas densities and/or temperatures in AGN must be higher than around SB activity. We can clearly exclude higher (average) gas densities in AGN, as our LVG analysis yields quite 'low' gas densities of $n(\text{H}_2) < 10^{4.5} \text{ cm}^{-3}$ in the AGN sources. However, within the 30m beam, we potentially average over many giant molecular cloud complexes (GMCs) which could each actually be denser than their average, if, for instance, the GMC number density is not very high and lower than that in the SB sources. Thus, one explanation for the 'lower' average gas densities may be that the molecular gas traced by the HCN and HCO^+ emission does not split up into as many high density clumps/GMCs in our AGN sources as it seems to be the case in SB environments (compare Zhang et al. 2001; Alonso-Herrero et al. 2002; Wilson et al. 2003; Galliano et al. 2005).

An increased HCN abundance in AGN compared to SB environments could equally explain the observed differences in the line ratios. A chemical enhancement of HCN can be created in two different ways: either through far-ultraviolet radiation from O and B stars in young high-mass star forming regions (e.g., Tielens & Hollenbach 1985; Blake et al. 1987; Sternberg & Dalgarno 1995), or through strong X-ray (ir)radiation from an AGN (e.g., Lepp & Dalgarno 1996; Maloney et al. 1996). While UV radiation affects primarily the surfaces of gas clouds in the circumnuclear regions ($\leq 1 \text{ kpc}$), creating Photon Dissociation Regions (PDRs), X-rays penetrate deeply into the circumnuclear disk (CND), forming huge X-ray Dissociation Regions (XDRs). As a consequence of this volume versus surface effect, the X-ray radiation from the AGN might thereby produce higher HCN abundances relative to CO than the UV radiation of SBs which may explain the significantly higher HCN-to- $\text{CO}(J=1-0)$ luminosity ratios found in AGN (e.g., Kohno et al. 2001; Usero et al. 2004; Imanishi et al. 2006; Graciá-Carpio et al. 2006). This scenario seems to be consistent with the estimated abundance ratios in our sample. They appear to be higher in the AGN than in the SB dominated sources in our sample.

Alternatively, the CO abundance might be smaller in AGN than around SB activity either because of oxygen depletion (e.g., Sternberg et al. 1996; Shalabiea & Greenberg 1996) or the influence of X-rays from the AGN (e.g. Meijerink & Spaans 2005). This could also result in the apparently higher HCN-to-CO ratios in AGN. The oxygen depletion has, however, been already ruled out for the XDR in NGC 1068 because it would produce different HCO^+ -to-HCN($J=1-0$) ratios than observed (e.g., Usero et al. 2004; Kohno et al. 2005). On the other hand, at the presence of a strong X-ray radiation field, CO dissociation may occur more frequently predicting similar HCO^+ -to-HCN intensity ratios to those observed in NGC 1068 and NGC 5194 and eventually also a decreased CO abundance (e.g. Meijerink & Spaans 2005). This scenario can neither be supported nor discarded with our current data and has to be investigated further.

Supernovae explosions (SNe), or more generally, ionisation effects from cosmic rays (e.g., Dickinson et al. 1980; Wooten 1981; Nguyen et al. 1992; Wild et al. 1992), are suspected to significantly increase the HCO^+ abundance while potentially decreasing the HCN abundance, yielding thus higher HCO^+ -to-HCN intensity ratios in evolved SBs (higher frequency of SNe) than in AGN. The most prominent examples for the role of the evolutionary stage of a SB are M82 and NGC 253; the starburst in NGC 253 is supposed to be in an evolutionary stage prior to that one in M82 and its molecular gas appears to be mainly dominated by shocks (e.g., Martín et al. 2006) rather than PDRs/SNe in contrast to M82 (e.g., García-Burillo et al. 2002). The HCO^+ -to-HCN intensity ratio is observed to be significantly lower in NGC 253 than in the PDR of M82 (see Fig. 5). In this context, the results obtained on the HCN and HCO^+ abundances in the evolved SB, PDR-dominated M82 are in excellent agreement with what is expected from theoretical predictions; M82 shows a very low $[\text{HCN}]/[\text{HCO}^+]$ abundance ratio of ≤ 1 . This may also explain the difference to the other SB sources in our sample who may all be in an earlier SB phase than M82, and emphasize the dependence of the excitation and chemistry on the evolutionary stage of the SB, whether reflected in more pronounced shocks or PDRs/SNe dominance. This is of particular importance as it sets tight constraints on the comparison to AGN dominated sources.

As a further alternative, dust heating, coupled to gas density and caused by the UV/X-ray radiation of the AGN, together with infrared (IR) radiative pumping could also be the origin of the stronger HCN emission in XDRs although, if true, a tighter correlation of the HCN luminosity with the IR luminosity than with the FIR luminosity would be expected as well as a strong correlation between the IR and X-ray luminosity. Such correlations have not yet been found (e.g., Lutz et al. 2004; Gao & Solomon 2004a,b) but X-ray absorption in compton thick sources and variability effects might lead to a large scatter in the data used so far, thus washing out possible correlations. However, IR pumping should similarly affect the HCN and HCO^+ emission, which both have vibrational modes at similar wavelengths of 12-14 μm , as recently discussed by (Guélin et al. 2007). Thus, HCO^+ -to-HCN ratios close to unity would be expected, in case IR pumping is significant, implying that

non-collisional excitation of HCN and HCO^+ in sources with low HCO^+ -to-HCN ratios cannot be a dominant process. Also, the HCO^+ -to-HCN intensity ratios in the AGN sources even decrease with increasing J ; this would not be expected if IR pumping were significant. However, recent observations of the HNC emission in some ULIRGs and a high redshift quasar (e.g., Aalto et al. 2007; Guélin et al. 2007) indicate that IR pumping may well be a significant factor in the excitation of at least HNC in sources with compact IR nuclei, but HNC (its vibrational state is at 24 μm) seems to be more easily excitable through IR pumping than HCN and HCO^+ (e.g., Aalto et al. 2007; Guélin et al. 2007). HNC observations of our sample will be discussed in a future paper.

We note that, although the statistics in our sample may be still small, especially for the AGN sources, the trend of different line ratios between AGN and SB dominated sources, seen in our data, is very pronounced and also further supported by literature data. Not only fall sources such as NGC 253 and NGC 4569 in the same line ratio regions as our SB sources, but the results on the AGN sources are also encouraged by recent results on the center of NGC 6951 (Krips et al. 2007) as well as that on NGC 1097 and NGC 5033 (e.g. Kohno 2005; Kohno, Nakanishi, & Imanishi 2007). However, more AGN dominated galaxies in our sample would certainly be beneficial to substantiate our results.

6.2. Comparison to theoretical results

The lower gas densities in our AGN sources may actually resolve a 'conflict' introduced by recent theoretical studies (Meijerink & Spaans 2005; Meijerink et al. 2006, 2007) on XDR and PDR environments. While these authors claim that the HCO^+ -to-HCN intensity ratios are actually >1 in XDRs, we rather find *low* HCO^+ -to-HCN intensity ratios as opposed to their results. However, as emphasized in Meijerink et al. (2007), high HCO^+ -to-HCN intensity ratios are expected in high density regions, which does not seem to be the case for the 100 pc scale disks/regions in NGC 1068 and NGC 5194. For lower density regions, Meijerink et al (2007) indeed find low HCO^+ -to-HCN intensity ratios in agreement with our results. Also, their models predict higher surface temperatures in XDRs for strong X-ray radiations fields but low gas densities when compared to PDRs. This indicates a more efficient gas heating in XDRs than PDRs. The high kinetic temperatures resulting from our LVG analysis for the AGN sources fit nicely into this picture and are even more supported by recent results found in nearby AGN through the CO($J=3-2$) emission. Matsushita et al. (2005) detect stronger central emission through CO($J=3-2$) than through CO($J=1-0$) in their SMA sample of several nearby Seyfert galaxies. This may indicate that temperature effects play a non-negligible role for the high HCN-to-CO($J=1-0$) intensity ratios in AGN. This would also explain the decrease of the HCN-to-CO intensity ratios with increasing rotational number J in our sample for the AGN sources. However, we also find significantly different HCN abundances that may support an HCN enhancement through the strong X-ray radiation field in AGN in addition to a temperature effect.

6.3. Implication for the SFR - dense gas relation in galaxies

Gao & Solomon (2004a,b) find a strong correlation between the star formation rate (SFR), being proportional to the infrared luminosity, and the dense gas mass, traced by the HCN luminosity. However, the results on the AGN dominated galaxies of our sample may indicate that this correlation is violated in certain AGN environments (compare also Kohno, Nakanishi, & Imanishi 2007). The HCN-to-CO(J=1-0) ratios for NGC 1068, NGC 5194 and at the center of NGC 6951 (Krips et al. 2007) do not fall on the correlation of Gao & Solomon (2004a,b). This may be a consequence of the overabundance of HCN in the AGN sources of our sample. As a potential alternative, the HCN-to-CO ratios at higher transitions may be better suited for AGN environments than the HCN-to-CO(J=1-0) ratios as they seem to coincide with the SFR-HCN correlation.

7. SUMMARY AND CONCLUSIONS

We observed the centre of 12 nearby active galaxies in several transitions of HCN and HCO⁺ with the IRAM 30m telescope. The results can be summarised as follows:

- 1.) We find that the HCN intensity ratios vary significantly with activity type, i.e., depending on which power source dominates the central emission. The HCN ($R_{J_u, J_l/10}^{\text{HCN}}$), HCO⁺ ($R_{J_u, J_l/10}^{\text{HCO}^+}$) and HCO⁺-to-HCN ($R_{J_u, J_l/10}^{\text{HCO}^+/\text{HCN}}$) intensity ratios seem to increase with increasing SB contribution, in agreement with predictions from theoretical models. The highest intensity ratios are found in the evolved PDR-dominated starburst galaxy M82 while the lowest ratios are found in NGC 1068, a pure AGN source with a potential central XDR.
- 2.) We also find a variation in the intensity ratios among the starburst sources of our sample which may be explained by the evolutionary phase of the starburst, i.e., a differing dominance of shocks (pre-SB), hot cores (young SB), PDRs and SNe/cosmic rays (evolved SB).
- 3.) An LVG analysis of the HCN and HCO⁺ data suggests that the SB dominated sources in our sample have high molecular gas densities around $n(\text{H}_2) \approx 10^{4.0} - 10^{6.5} \text{ cm}^{-3}$, kinetic gas temperatures of $T_k \approx 20 - 120 \text{ K}$ and HCN abundances of $Z(\text{HCN}) \approx (0.001 - 2) \times 10^{-8}$, while the AGN dominated regions seem to show $n(\text{H}_2) \leq 10^{4.5} \text{ cm}^{-3}$ and temperatures of $T_k > 40 \text{ K}$ with HCN abundances of $Z(\text{HCN}) \approx (0.1 - 10) \times 10^{-7}$.
- 4.) The low HCO⁺-to-HCN intensity ratios found in the AGN sources of our sample seem to make it un-

likely that non-collisional excitation plays a significant role in AGN for the HCN and HCO⁺ emission. This may be further supported by the *decreasing* HCO⁺-to-HCN intensity ratios with increasing rotational number J in the AGN sources of our sample.

- 5.) Assuming thus purely collisional excitation in AGN, we can exclude gas density effects as main cause for the higher HCN-to-CO(J=1-0) ratios found in AGN favorising hence an increased HCN abundance and/or temperature effects in AGN. The latter is supported by decreasing HCN-to-CO ratios with increasing rotational number J.
- 6.) To explain the potential differences in gas densities between AGN and SB environments of our sample, we favor a scenario in which the molecular gas may be either significantly less clumpy, i.e., has a lower 'clump/GMC number density' in AGN than SB environments or, alternatively, is more continuously smeared over AGN environments, i.e., has indeed a lower gas density.
- 7.) An estimate of the dense molecular mass to HCN luminosity ($M_{\text{H}_2\text{-to-L}_{\text{HCN}}}$) conversion factor $X(\text{HCN})$ results in $X(\text{HCN}) = 10_{-7}^{+10} M_{\odot} (\text{K km s}^{-1} \text{ pc}^2)^{-1}$ for the AGN sources in our sample. This is a factor of ~ 2 lower than that found by Solomon, Downes & Radford (1992); Greve et al. (2007) for ULIRGs and starburst sources of $X(\text{HCN}) = 20_{-10}^{+30} M_{\odot} (\text{km s}^{-1} \text{ pc}^2)^{-1}$, but consistent with the value favored by Gao & Solomon (2004a) for their sample of nearby active galaxies and ULIRGs.
- 8.) The overabundance of HCN found in the AGN sources of our sample indicates that the correlation between SFR and HCN luminosity may be violated in the vicinity of an AGN. Given the decreasing nature of the HCN-to-CO ratio with increasing transition, we suggest to use the J=3-2 transition of HCN and CO as an alternative.

The results in this paper are based on observations carried out with the IRAM 30m telescope in Spain. IRAM is supported by INSU/CNRS (France), MPG (Germany) and IGN (Spain). We are grateful to the dedicated staff at the IRAM 30m telescope who have been very supportive and helpful during the observations. We thank the anonymous referee for very helpful suggestions on improving the paper.

REFERENCES

- Alonso-Herrero, Almudena; Rieke, George H.; Rieke, Marcia J.; Scoville, Nick Z., 2002, AJ, 124, 166
Aalto, S.; Spaans, M.; Wiedner, M. C.; Hüttemeister, S., 2007, A&A, 464, 193
Boer, B.; Schulz, H., 1993, A&A, 277, 397
Blake, G.A.; Sutton, E. C.; Masson, C. R.; Phillips, T. G., 1987, ApJ, 315, 621
Bryant, Peter M.; Scoville, Nick Z., 1999, AJ, 117, 2632
Dahlem, M.; Heckman, T. M.; Fabbiano, G.; Lehnert, M. D.; Gilmore, D., 1996, ApJ, 461, 724

- Dickinson, D. F.; Dinger, A. S. C.; Kuiper, T. B. H.; Rodriguez Kuiper, E. N., 1980, *ApJ*, 237, L43
- Downes, D., & Eckart, A., 2007, *A&A*, 468, L57
- Galliano, E.; Alloin, D.; Pantin, E.; Lagage, P. O.; Marco, O., 2005, *A&A*, 438, 803
- Gao, Yu; Solomon, Philip M., 2004a, *ApJS*, 152, 63
- Gao, Yu; Solomon, Philip M., 2004b, *ApJ*, 606, 271
- García-Burillo, S.; Graciá-Carpio, J.; Guélin, M.; Neri, R.; Cox, P.; Planesas, P.; Solomon, P. M.; Tacconi, L. J.; Vanden Bout, P. A., 2006, *ApJ*, 645, L17
- García-Burillo, S.; Martín-Pintado, J.; Fuente, A.; Usero, A.; Neri, R., 2002, *ApJ*, 575, L55
- Greve, A.; Neininger, N.; Sievers, A.; Tarchi, A., 2006, *A&A*, 459, 441
- Greve, T. R.; Papadopoulos, P. P.; Gao, Y.; Radford, S. J. E., 2006, *astro-ph/10378*
- Graciá-Carpio, J.; García-Burillo, S.; Planesas, P.; Colina, L., 2006, *ApJ*, 640, L135
- Greenawalt, B.; Walterbos, R. A. M.; Thilker, D.; Hoopes, C. G., 1998, *ApJ*, 506, 135
- Guélin, M.; Salomé, P.; Neri, R.; Graciá-Carpio, J.; Cernicharo, J.; Cox, P.; Planesas, P.; Solomon, P. M.; Tacconi, L. J.; vanden Bout, P., 2007, *A&A*, 462, L45
- Haas, M.; Klaas, U.; Müller, S.A.H.; Chini, R.; Coulson, I., 2001, *A&A*, 367, L9
- Ho, L.C.; Filippenko, A.V.; Sargent, W.L.W., 1997, *ApJS*, 112, 315
- Iono, D.; Wilson, C.; Takakuwa, S.; Yun, M.; Petitpas, G.; Peck, A.; Ho, P.; Matsushita, S.; Pihlstrom, Y.; Wang, Z., [arXiv:astro-ph/0701123](https://arxiv.org/abs/0701123)
- Imanishi, M.; Nakanishi, K.; Kohno, K., 2006, *AJ*, 131, 2888
- Kohno, K.; Nakanishi, K.; Imanishi, M., 2007, Conference proceedings to appear in "The Central Engine of Active Galactic Nuclei", ed. L. C. Ho and J.-M. Wang (San Francisco: ASP), *astro-ph/07042818*
- Kohno, K., The evolution of star bursts: The 331st Wilhelm and Else Heraeus Seminar, AIP Conference Proceedings, 2005, Volume 783, p. 203
- Kohno, K., proc. of the IAU 8th APRM, Vol.I, held 2-5 July 2002 at Tokyo, Japan. ASP Conf. Proc., Vol. 289. Ed.: S. Ikeuchi, J. Hearnshaw and T. Hanawa, 2003, p.349
- Kohno, K.; Matsushita, S.; Vila-Vilaró, B.; Okumura, S. K.; Shibatsuka, T.; Okiura, M.; Ishizuki, S.; Kawabe, R., The Central kpc of Starbursts and AGN; ASP Conf. Proc., Vol. 249. Ed.: J. H. Knapen, J. E. Beckman, I. Shlosman, and T. J. Mahoney, 2001, p.672
- Kohno, K.; Kawabe, R.; Vila-Vilaró, B., 1999, *ApJ*, 511, 157
- Komossa, S.; Burwitz, V.; Hasinger, G.; Predehl, P., 2003, *ANS*, 324, 33
- Krips, M.; Neri, R.; García-Burillo, S.; Combes, F.; Schinnerer, E.; Baker, A.J.; Eckart, A.; Boone, F.; Hunt, L.; Leon, S.; Tacconi, L.J., 2007, *A&A*, 468, L63
- Kronberg, P.P.; Biermann P.; Schwab F.R., 1981, *ApJ*291, 693
- Lepp, S.; Dalgarno, A., 1996, *A&A*, 306, 21
- Lutz, D.; Maiolino, R.; Spoon, H. W. W.; Moorwood, A. F. M., 2004, *A&A*, 418, 465
- Maloney, Philip R.; Hollenbach, David J.; Tielens, A.G.G.M., 1996, *ApJ*, 466, 561
- Marco, O.; & Brooks, K. J., 2003, *A&A*, 398, 101
- Martín, S.; Mauersberger, R.; Martín-Pintado, J.; Henkel, C.; García-Burillo, S., 2006, *ApJS*, 164, 450
- Matsushita, S.; Mao, R.-Q.; Muller, S.; Chou, C.-Y.; Satoko, S.-S.; Dinh-van-Trung; Lim, J.; Hsieh, P.-Y.; Peck, A. B., 2005, *JKAS*, 38, 169
- Matsushita, S.; Kawabe, R.; Matsumoto, H.; Tsuru, T.G.; Kohno, K.; Morita, K.-I.; Okumura, S.K.; 2000, *ApJ*, 545, L107
- Matsushita, S.; Kohno, K.; Vila-Vilaro, B.; Tosaki, T.; Kawabe, R., 1998, *ApJ*, 495, 267
- Meijerink, R.; Spaans, M.; Israel, F. P., 2007, *A&A*, 461, 793
- Meijerink, R.; Spaans, M.; Israel, F. P., 2006, *ApJ*, 650, L103
- Meijerink, R.; Spaans, M., 2005, *A&A*, 436, 397
- Nakanishi, K.; Okumura, S.K.; Kohno, K.; Kawabe, R.; Nakagawa, T., 2005, *PASJ*, 57, 575
- Nguyen, Q.-R.; Jackson, J.M.; Henkel, Ch.; Truong, B.; Mauersberger, R., 1992, *ApJ*, 399, 521
- Nguyen-Rieu, Viallefond, F., Combes, F., Jackson, J. M., Lequeux, J., Radford, S., 'Astronomy with Millimeter and Submillimeter Wave Interferometry', IAU Colloquium 140, ASP Conference Series, Vol. 59, 1994, editors: M. Ishiguro and J. Welch, Eds., p.336
- Patruno, A.; Portegies Zwart, S.; Dewi, J.; Hopman, C., 2006, *MNRAS*, 370, L6
- Pisano, D. J.; Wilcots, Eric M.; 2000, *MNRAS*, 319, 821
- Risaliti, G.; Maiolino, R.; Marconi, A.; Sani, E.; Berta, S.; Braito, V.; Ceca, R. Della; Franceschini, A.; Salvati, M., 2006, *MNRAS*, 365, 303
- Sanders, D. B.; Soifer, B. T.; Elias, J. H.; Madore, B. F.; Matthews, K.; Neugebauer, G.; Scoville, N. Z., 1988, *ApJ*, 325, 74
- Sakamoto, K.; Scoville, N. Z.; Yun, M. S.; Crosas, M.; Genzel, R.; Tacconi, L. J., 1999, *ApJ*, 514, 68
- Sauvage, M.; Blommaert, J.; Boulanger, F.; Cesarsky, C. J.; Cesarsky, D. A.; Desert, F. X.; Elbaz, D.; Gallais, P.; Joncas, G.; Metcalfe, L.; Okumura, K.; Ott, S.; Siebenmorgen, R.; Starck, J. L.; Tran, D.; Vigroux, L., 1996, *A&A*, 315, 89
- Shalabiea, O. M., & Greenberg, J. M. 1996, *A&A*, 307, 52
- Schinnerer, E.; Bker, T.; Emsellem, E.; Downes, D., 2007, *A&A*, 462, L27
- Schinnerer, E.; Eckart, A.; Tacconi, L. J.; Genzel, R.; Downes, D., 2000, *ApJ*, 533, 850
- Schulz, A.; Güsten, R.; Köster, B.; Krause, D., 2001, *A&A*, 371, 25
- Solomon, P. M.; Downes, D.; Radford, S. J. E., 1992, *ApJ*, 387, L55
- Solomon, P. M.; Radford, S. J. E.; Downes, D., 1990, *ApJ*, 348, L53
- Sternberg, A., Yan, M., and Dalgarno, A. 1996, in *Molecules in Astrophysics: Probes and Processes*, ed. E. F. van Dishoeck (Dordrecht: Kluwer), IAU Symp., 178, 141
- Sternberg, A., & Dalgarno, A., 1995, *ApJS*, 99, 565
- Sternberg, A.; Genzel, R.; Tacconi, L., 1994, *ApJ*, 436, L131
- Tacconi, L. J.; Genzel, R.; Tecza, M.; Gallimore, J. F.; Downes, D.; Scoville, N. Z., 1999, *ApJ*, 524, 732
- Tacconi, L. J., Genzel, R., Blietz, M., Cameron, M., Harris, A. I., & Madden, S., 1994, *ApJ*, 426, 77
- Thronson, H.A., Jr.; Rubin, H.; Ksir, A., 1991, *MNRAS*, 252, 550
- Tielens, A.G.G.M.; Hollenbach, D., 1985, *ApJ*, 291, 747
- Usero, A.; García-Burillo, S.; Fuente, A.; Martín-Pintado, J.; Rodríguez-Fernández, N. J., 2004, *A&A*, 419, 897
- Wang, M.; Henkel, C.; Chin, Y.-N.; Whiteoak, J. B.; Hunt Cunningham, M.; Mauersberger, R.; Muters, D., 2004, *A&A*, 422, 883
- Wild, W., Harris, A. I., Eckart, A., et al. 1992, *A&A*, 265, 447
- Wilson, C. D.; Scoville, N.; Madden, S.C.; Charmandaris, V., 2003, *ApJ*, 599, 1049
- Weiß, A.; Downes, D.; Neri, R.; Walter, F.; Henkel, C.; Wilner, D. J.; Wagg, J.; Wiklind, T. 2007, *A&A*, 467, 955
- Weiß, A.; Walter, F.; Neininger, N.; Klein, U., 1999, *A&A*, 345, L23
- Wootten, A., 1981, *ApJ*, 245, 105
- Zhang, Qing; Fall, S. Michael; Whitmore, Bradley C., 2001, *ApJ*, 561, 727

TABLE 1
BASIC PROPERTIES OF THE SAMPLE.

Source	z	RA	Dec	Type ^a
NGC1068	0.0038	02:42:40.7	-00:00:47.9	AGN
NGC5194	0.0015	13:29:52.7	+47:11:42.6	AGN
NGC4826	0.0014	12:56:43.8	+21:40:58.9	AGN+SB?
NGC3627	0.0024	11:20:15.0	+12:59:29.5	AGN+SB
NGC4569	0.0008	12:36:49.8	+13:09:46.3	AGN+SB
NGC6951	0.0047	20:37:14.5	+66:06:19.7	AGN+SB
NGC6946	0.0002	20:34:52.3	+60:09:14.2	SB
NGC2146	0.0031	06:18:37.7	+78:21:25.3	SB
M82	0.0007	09:55:52.2	+69:40:46.9	SB
NGC6240	0.0245	16:52:58.9	+02:24:03.4	ULIRG(AGN+SB)
Mrk231	0.0422	12:56:14.2	+56:52:25.2	ULIRG(AGN+SB)
Arp220	0.0181	15:34:57.1	+23:30:11.5	ULIRG(AGN+SB)

^a type of activity found in the central $\pm 15''$. AGN denotes thereby Seyfert or LINER galaxies. Please note that NGC 1068 for instance also contains a SB ring but on much larger scales (i.e., $\sim \pm 20''$). NGC 6951 also houses a strong SB which is still within the 30m beam as opposed to NGC 1068. Most classifications are from the NED; composite nature (AGN+SB): NGC 3627 (Dahlem et al. 1994(@); NGC 4569 (Gabel et al. 2002); NGC 4826 (García-Burillo et al. 2003); NGC 6951 (see text); NGC 6240 (Tecza et al. 2000; Gallimore & Beswick 2004); Mrk231 (Smith et al. 1999).

TABLE 2
OBSERVATIONAL PARAMETERS AS
TAKEN FROM THE IRAM 30M
HOMEPAGE.

Observed Frequency	F _{eff}	B _{eff}	θ_{beam} ($''$)
89 GHz	0.95	0.78	29.5
177 GHz	0.93	0.65	14.0
267 GHz	0.88	0.46	9.5

TABLE 3
LINE PARAMETERS FOR THE HCN AND HCO⁺ DATA.

Source	I_{10}^{HCN} ^a K km s ⁻¹	I_{21}^{HCN} ^a K km s ⁻¹	I_{32}^{HCN} ^a K km s ⁻¹	Δv ^b km s ⁻¹	θ_s^{10c} [$''$]	θ_s^{21c} [$''$]	θ_s^{32c} [$''$]	f_{10}^d	f_{21}^d	f_{32}^d
NGC1068	24.5±0.9	20.0±0.4	19.0±0.6	220±10	4.5	3.0	3.0	0.09	0.16	0.29
NGC5194	4.7±0.2	2.2±0.6	<2.0	120±10	15	10	10	0.53	0.67	0.83
NGC4826	6.0±0.4	4.7±0.4	3.4±0.4	300±20	20	20	20	0.67	0.91	0.91
NGC3627	2.7±0.2	<2.0	<3.0	290±30	8	8	8	0.23 ^f	0.56 ^f	0.71 ^f
NGC4569	2.8±0.1	2.6±0.4	2.3±0.5	210±30	10	10	10	0.32 ^f	0.67 ^f	0.83 ^f
NGC6951	3.1±0.1	5.0±0.7	3.6±1.0	300±20	17	17	17	0.59	0.83	0.91
NGC6946	9.9±0.1	11.3±0.6	9.2±0.6	150±5	10	10	10	0.32 ^f	0.67 ^f	0.83 ^f
NGC2146	5.0±0.1	4.4±0.3	4.3±0.4	290±10	20	20	20	0.67 ^f	0.91 ^f	0.91 ^f
M82 ^e	29±0.2	26±0.6	27±1	130±5	—	—	—	1	1	1
NGC6240	3.2±0.2	8.8±0.3	12.3±0.8	410±20	3	3	3	0.07	0.24	0.42
Mrk231	1.9±0.1	4.9±1.0	9.3±0.6	220±20	3	3	3	0.04	0.16	0.29
Arp220	9.7±0.4	28.4±0.7	43.0±1.0	530±20	2	2	2	0.02	0.08	0.15
	$I_{10}^{\text{HCO}^+}$ ^a K km s ⁻¹	$I_{32}^{\text{HCO}^+}$ ^a K km s ⁻¹	Δv ^b K km s ⁻¹	same as above						
NGC1068	14.6±0.2	7.6±0.8	234±4							
NGC5194	2.4±0.1	<1.3	134±7							
NGC4826	3.5±0.1	<2.5	300±30							
NGC3627	2.7±0.2	<2.1	230±15							
NGC4569	2.3±0.2	<2.1	211±17							
NGC6951	2.2±0.1	<2.9	300±20							
NGC6946	8.5±0.1	8.6±0.6	150±3							
NGC2146	6.3±0.2	5.2±0.6	300±20							
M82	40.2±0.2	34.0±2.0	130±10							
NGC6240	5.0±0.5 ^g	8.0±1.0 ^g	—							
Mrk231	1.6±0.2 ^g	3.8±0.4 ^g	—							
Arp220	4.6±0.5 ^g	8.8±0.9 ^g	—							

^a Velocity integrated intensities, not yet corrected for filling factors; for a definition see equation 2. Error are purely statistical and were determined from the gaussian line fits to the data.

^b FWHM of HCN and HCO⁺ line.

^c Most of the source sizes have been determined either from the HCN maps where accesible (e.g., NGC 6951: Krips et al. 2007b) or from CO maps (NUGA project: García-Burillo et al. 2004; BIMA-SONG: Helfer et al. 2003). Individual galaxies not found in the BIMA SONG or NUGA survey: NGC 2146 (Greve et al. 2006); Mrk231, Arp220 (Downes & Solomon 1998); NGC 6946 (Schinnerer et al. 2007); NGC 6240 (Iono et al. 2007).

^d For a definition see Equation 3. While for the first one the major axis (FWHM) of the emission was chosen, the minor axis was taken for the elliptical case.

^e All HCN and HCO⁺ lines were averaged over the same area of 30 $''$ so that they all should have the same filling factor assuming that they come from the same emission region. However, it is not unprobable that the higher-J HCN and HCO⁺ lines originate from a more compact region than the HCN(J=1-0) and HCO⁺(J=1-0) line emission but this would make the ratios listed in Table 4 for M82 even higher.

^f We assumed elliptical source sizes for the filling factor here (see definition in Equation 3). The minor axis of the emission was taken for the source size.

^g HCO⁺ data taken from Graciá-Carpio et al. 2006. We assumed a 10% error for the integrated intensities here.

TABLE 4
INTENSITY AND LUMINOSITY RATIOS.

Source	$R_{21/10}^{\text{HCN a}}$	$R_{32/10}^{\text{HCN a}}$	$R_{32/10}^{\text{HCO}^+ \text{ a}}$	$R_{10/10}^{\text{HCO}^+/\text{HCN a}}$	$R_{32/32}^{\text{HCO}^+/\text{HCN a}}$
NGC1068	0.44±0.02	0.21±0.01	0.14±0.02	0.60±0.01	0.38±0.07
NGC5194	0.3±0.1	<0.23	<0.2	0.72±0.06	<0.7
NGC4826	0.38±0.04	0.23±0.01	<0.3	0.59±0.04	<0.7
NGC3627	<0.4	<0.4	<0.3	1.0±0.1	<0.7
NGC4569	0.5±0.1	0.4±0.2	<0.4	0.85±0.07	<0.9
NGC6951	0.7±0.1	0.4±0.1	0.44±0.02	0.70±0.05	<0.8
NGC6946	0.64±0.05	0.42±0.03	0.45±0.03	0.86±0.03	0.94±0.08
NGC2146	0.67±0.04	0.57±0.05	0.51±0.06	1.30±0.08	1.2±0.2
M82 (aver) ^b	0.88±0.04	0.92±0.07	0.96±0.05	1.40±0.10	1.30±0.10
M82 (ePDR) ^b	1.00±0.06	1.00±0.10	1.10±0.10	1.40±0.10	1.20±0.30
M82 (centre) ^b	0.70±0.1	0.50±0.05	0.40±0.10	1.50±0.04	1.30±0.10
NGC6240	0.67±0.05	0.45±0.04	0.19±0.07 ^c	1.60±0.20 ^c	0.70±0.20 ^c
Mrk231	0.62±0.07	0.58±0.05	0.30±0.10 ^c	0.87±0.09 ^c	0.40±0.10 ^c
Arp220	0.69±0.03	0.50±0.02	0.21±0.06 ^c	0.48±0.05 ^c	0.20±0.05 ^c
LITERATURE DATA					
NGC253 ^d	–	<0.7	0.9±0.2	0.8±0.1	>1.0
IC342 ^e	0.8±0.05	0.4±0.04	–	0.9±0.1	–
NGC4945 ^f	–	0.7±0.1	0.4±0.1	1.1±0.1	0.7±0.1

^a corrected for beam filling effects using Equation 1 (see also Table 3).

^b Intensity ratios of M82 averaged over the entire disk (\equiv aver), at the position ($\equiv(+12'',+8''$) of the eastern PDR (\equiv ePDR) and at the center ($\equiv(0'',0''$). The ratios for the eastern PDR are given because of consistency reason.

^c HCO⁺ values taken from Graciá-Carpio et al. 2006.

^d SB galaxy. Data taken from Martin et al. in (prep.?).

^e SB galaxy. Data taken from Nguyen et al. (1994) and Schulz et al. (2001).

^f SB galaxy. taken from Wang et al. (2004)

TABLE 5
INTENSITY AND LUMINOSITY RATIOS.

Source	$R_{21/10}^{\text{CO}}$ ^a	$\frac{L_{\text{HCN}10}}{L_{\text{CO}10}}$ ^b	$\frac{L_{\text{HCN}21}}{L_{\text{CO}21}}$ ^b	$\frac{L_{\text{HCN}32}}{L_{\text{CO}32}}$ ^b
NGC1068	0.4	1.9	1.1	0.5
NGC5194	0.6	0.5	0.2	<0.3
NGC4826	0.5	0.4	0.3	-
NGC3627	0.6	0.1	<0.1	<0.1
NGC4569	0.6	0.2	0.1	-
NGC6951	0.7	0.2	0.2	-
NGC6946	0.4	0.2	0.3	0.3
NGC2146	0.3	0.01	0.02	0.03
M82	0.9	0.2	0.2	0.1
NGC6240	0.3	0.1	0.1	-
Mrk231	0.1	0.1	0.3	-
Arp220	0.2	0.1	0.3	0.3

^a corrected for beam filling effects using Equation 1 (see also Table 3).

^b CO luminosities were taken from IRAM 30m observations of NGC 3627, NGC 4569, NGC 4826 and NGC 6951 in context of the NUGA project. The CO(1-0) and CO(2-1) fluxes for NGC 1068 were derived from interferometric maps (taken from Schinnerer et al. 2000 and Krips et al., 2007a) while the CO(3-2) emission has been taken with APEX during its commissioning which is consistent with published values. The rest has been taken from the literature: Arp220 and Mrk231 from Radford et al. 1991 (CO(1-0) and CO(2-1)) and Narayanan et al. 2005 (CO(3-2)); NGC 6240 from Solomon et al. 1997 (CO(1-0)) and Tacconi et al. 1999 (CO(2-1)); NGC 2146 and NGC 6946 from Gao & Solomon 2004a (CO(1-0)), Braine et al. 1993 (CO(2-1)), Casoli et al. 1991 (CO(2-1)) and Dumke et al. 2001 (CO(3-2)); NGC 5149 from Nakai et al. 1994 (CO(1-0) and CO(2-1)) and Dumke et al. 2001 (CO(3-2)); M82 from Walter et al. 2002 (CO(1-0)), Thuma et al. 2000, (CO(2-1)) and Dumke et al. 1994 (CO(3-2)). CO(3-2) data on NGC 3627 are from Petitpas et al. (2005).

TABLE 6
RESULTS OF THE LVG ANALYSIS IN DEPENDENCY OF THE DOMINANT ACTIVITY TYPE.

Example source	T_k ^a K	$n(\text{H}_2)$ ^b cm^{-3}	$N(\text{HCN})/(\text{dv})$ ^c $\text{cm}^{-2} \text{ km}^{-1} \text{ s}$	$Z(\text{HCN})/(\text{dv}/\text{dr})$ ^d $\text{km}^{-1} \text{ s pc}$	$[\text{HCN}]/[\text{HCO}^+]$ ^e
NGC1068	20	$10^{4.0} - 10^{4.5}$	$10^{15} - 10^{16}$	$10^{-8} - 10^{-7}$	50
	60-240	$10^{2.0} - 10^{4.5}$	$10^{13} - 10^{16}$	$10^{-8} - 10^{-6}$	10
NGC6951	20	$10^{4.5} - 10^{5.0}$	$10^{15} - 10^{17}$	$10^{-8} - 10^{-7}$	50
	20-120	$10^{4.0} - 10^{6.0}$	$10^{13} - 10^{16}$	$10^{-9} - 10^{-7}$	10
M82(aver)	60-100	$10^{5.0} - 10^{6.5}$	$10^{15} - 10^{16}$	$10^{-10} - 10^{-8}$	0.01-1
NGC6240	20-120	$10^{3.5} - 10^{4.5}$	$10^{15} - 10^{16}$	$10^{-7} - 10^{-6}$	10

^a Kinetic gas temperature.

^b H_2 density.

^c HCN column density.

^d HCN abundance per velocity gradient.

^e Abundance ratio between HCN and HCO^+ .

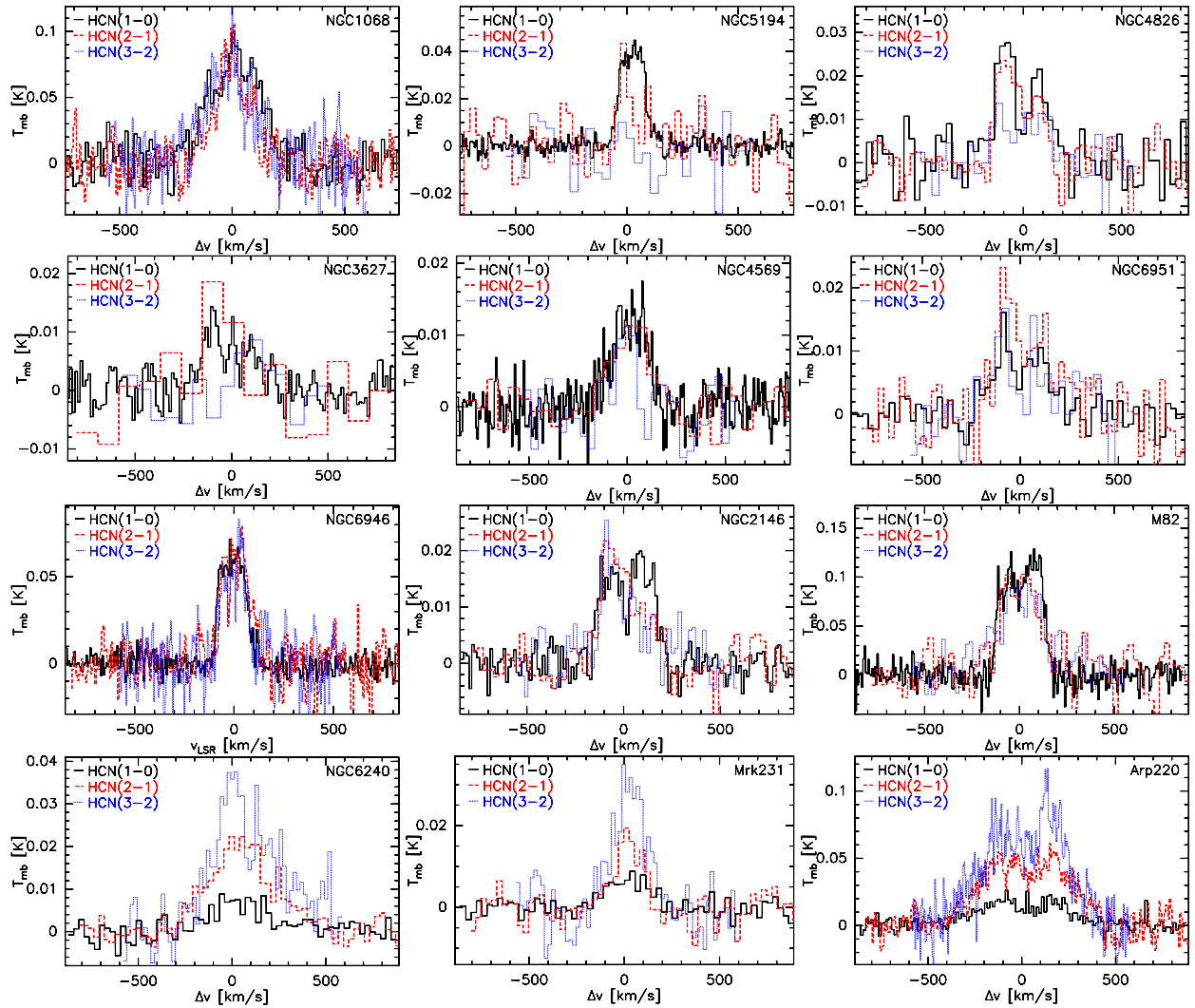


FIG. 1.— Line spectra of HCN($J=1-0$) (*solid black*), HCN($J=2-1$) (*dashed red*; please note that color figures are only available in the online version of the paper) and HCN($J=3-2$) (*dotted blue*) obtained at the centre of each of the 12 galaxies with the IRAM 30m telescope. The velocity scale is relative to the LSR velocity of the respective galaxy. Temperature scale is in main beam temperature (Kelvin) and has not been corrected for beam filling factors.

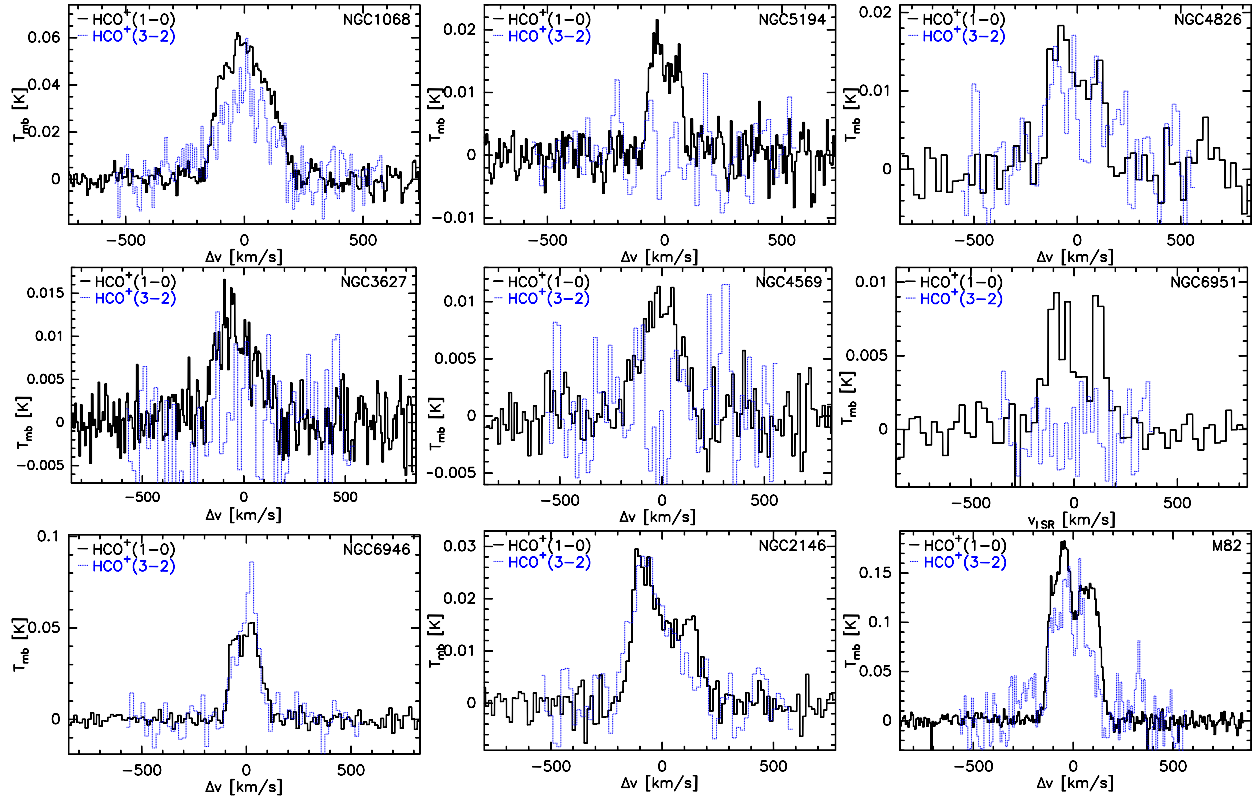


FIG. 2.— Line spectra of $\text{HCO}^+(J=1-0)$ (solid black) and $\text{HCO}^+(J=3-2)$ (dotted blue) obtained at the centre in 9 galaxies of our sample with the IRAM 30m telescope. The velocity scale corresponds to the LSR velocity of the respective galaxy. Flux scale is in main beam temperature (Kelvin) and has not been corrected for beam filling factors. The HCN and HCO^+ intensities of NGC 6240, Mrk231 and Arp220 were taken from Graciá-Carpio et al. (2006) and their spectra are thus not shown here.

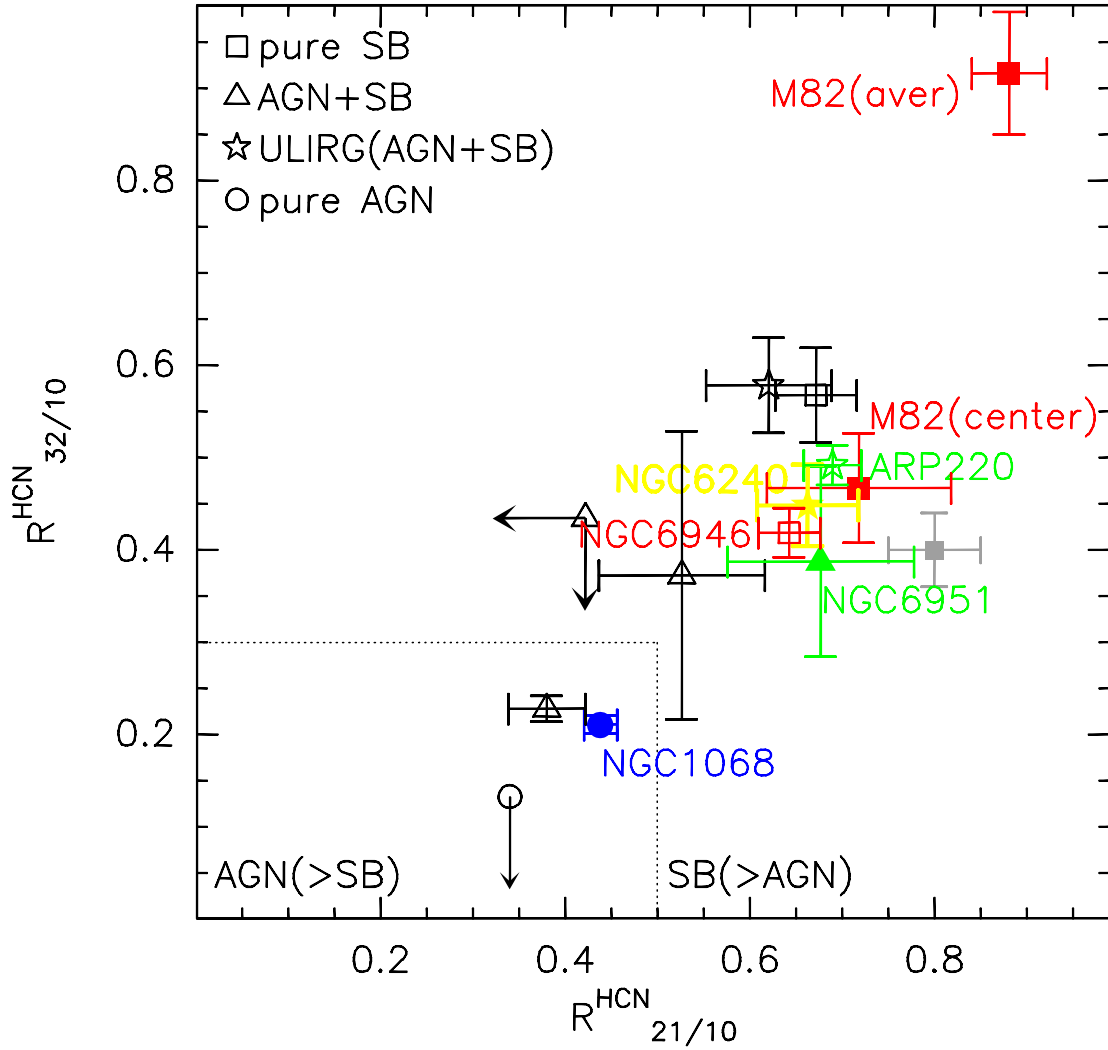


FIG. 3.— HCN($J=2-1$)-to- $\text{HCN}(J=1-0)$ and $\text{HCN}(J=3-2)$ -to- $\text{HCN}(J=1-0)$ intensity ratios of all 12 sources (this paper, Table 4) and IC 342 (filled grey box; data taken from the literature, Table 5). NGC 1068 (filled blue circle), NGC 6951 (filled green triangle), Arp220 (open green star), NGC 6240 (filled yellow star) and M82 (filled red box) are highlighted. The dotted grey lines should guide the readers eyes and indicate the putative different locations of the SB and AGN dominated sources in this diagram.

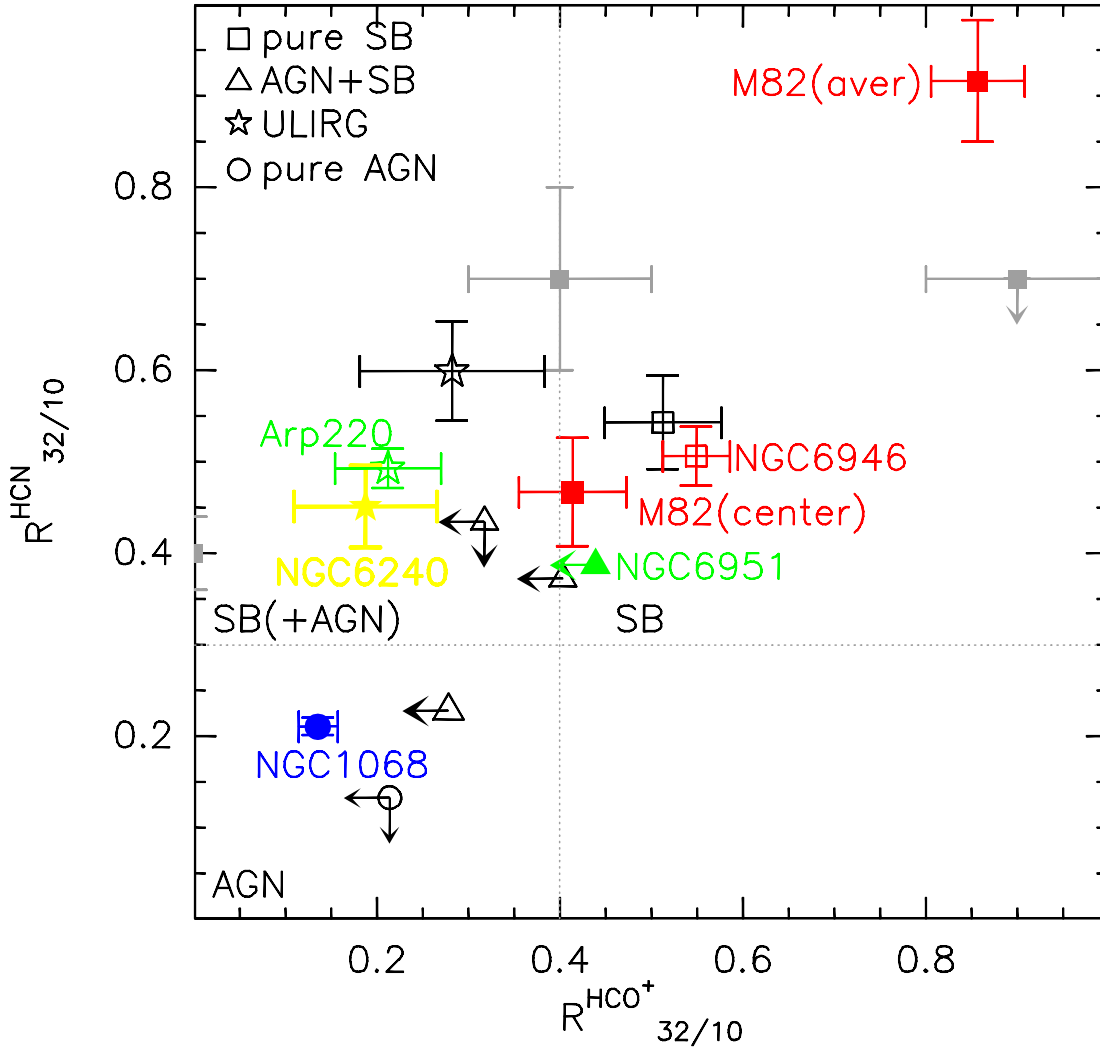


FIG. 4.— $\text{HCO}^+(J=3-2)$ -to- $\text{HCO}^+(J=1-0)$ and $\text{HCN}(J=3-2)$ -to- $\text{HCN}(J=1-0)$ intensity ratios of all 12 sources (this paper, Table 4) and NGC 253 and NGC 4945 (filled grey box; taken from the literature, Table 4). NGC 1068 (filled blue circle), NGC 6951 (filled green triangle), Arp 220 (open green triangle), NGC 6240 (filled yellow star) and M82 (filled red box) are highlighted. The dotted grey lines should guide the readers eyes and indicate the putative different locations of the SB and AGN dominated sources in this diagram.

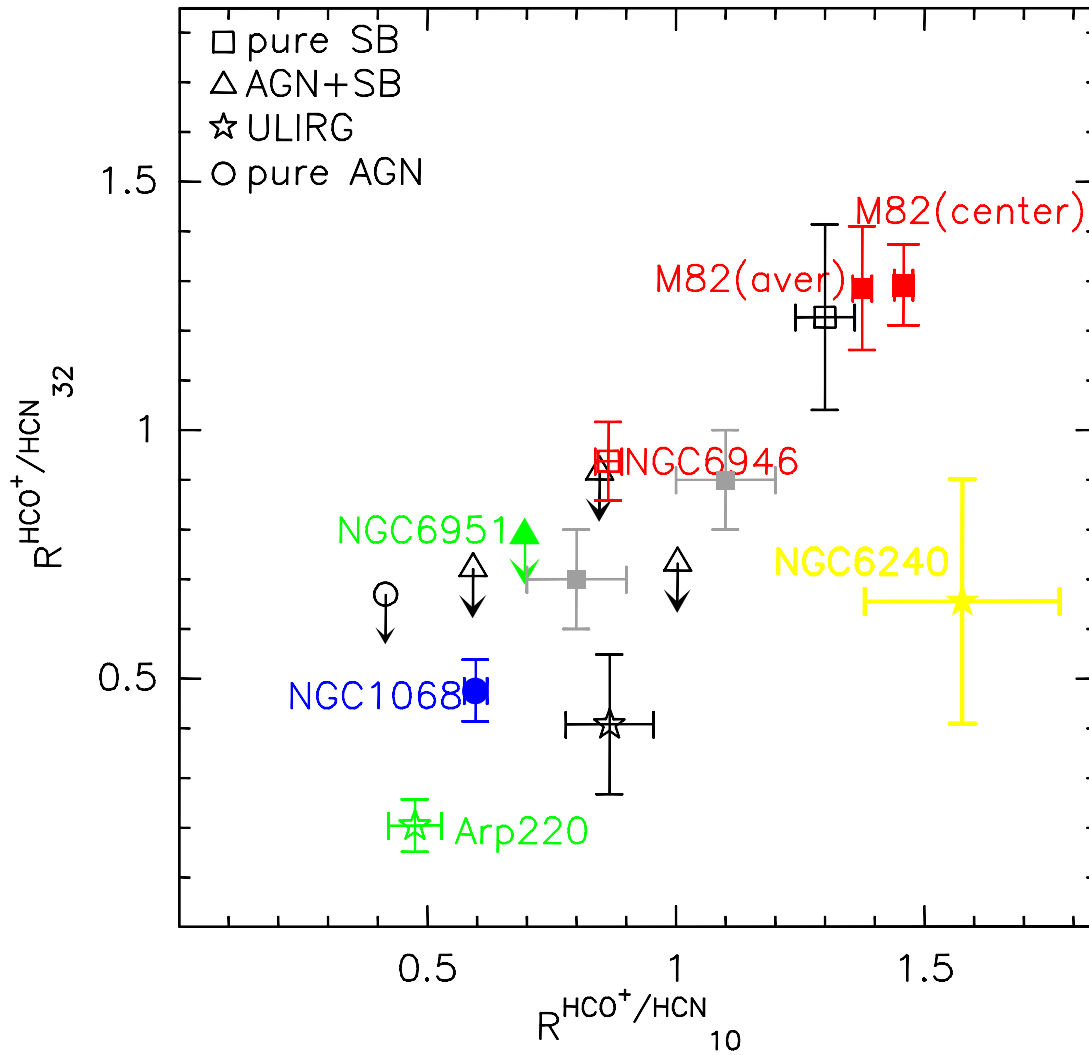


FIG. 5.— HCO^+ -to- $\text{HCN}(J=1-0)$ and HCO^+ -to- $\text{HCN}(J=3-2)$ intensity ratios of all 12 sources (this paper, Table 4) and NGC 253 and NGC 4569 (filled grey box; taken from the literature, Table 4). NGC 1068 (filled blue circle), NGC 6951 (filled green triangle), Arp220 (open green triangle), NGC 6240 (filled yellow star) and M82 (filled red box) are highlighted.

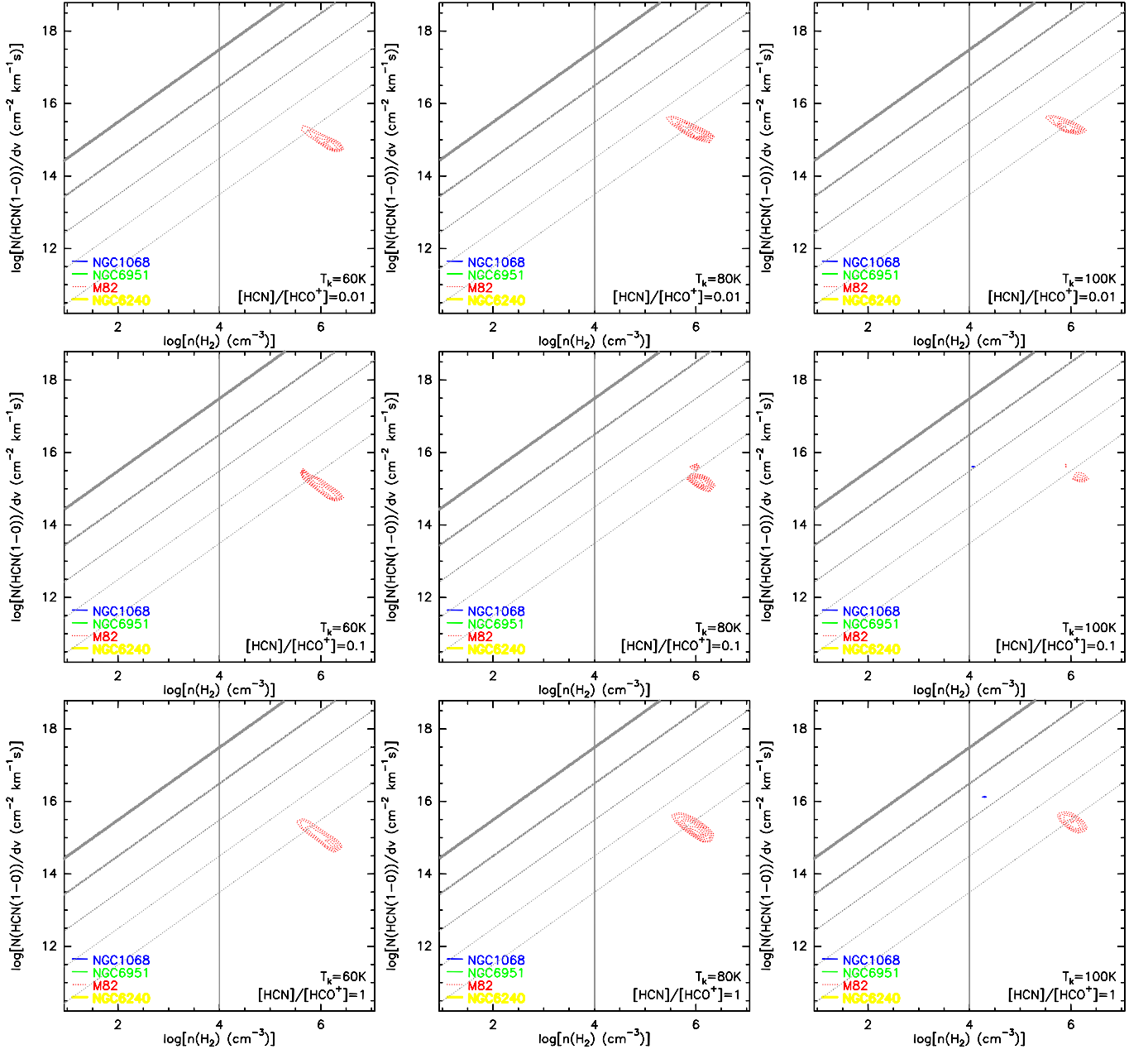


FIG. 6.— χ^2 -test results of the LVG analysis (see text for explanation) carried out with MIRIAD including the HCN and HCO⁺ data for different kinetic temperatures and abundance ratios of [HCN]/[HCO⁺]=0.01,0.1,1 (see also Fig. 7 for the higher abundance ratios of 10 & 50). The dotted red, solid blue, solid green and solid yellow contours correspond to M82, NGC 1068, NGC 6951 and NGC 6240 respectively. The area enclosed by the contours represent the lowest (reduced) χ^2 -test with $\chi^2 \leq 1$; for these low [HCN]/[HCO⁺] abundance ratios (i.e., ≤ 1) we only find a significant result for the SB dominated sources in our sample. The grey lines indicate $Z(\text{HCN})/(\text{dv}/\text{dr})$ with 10^{-5} , 10^{-6} , 10^{-7} , 10^{-8} and 10^{-9} km⁻¹ s pc (from top to bottom, decreasing in line thickness).

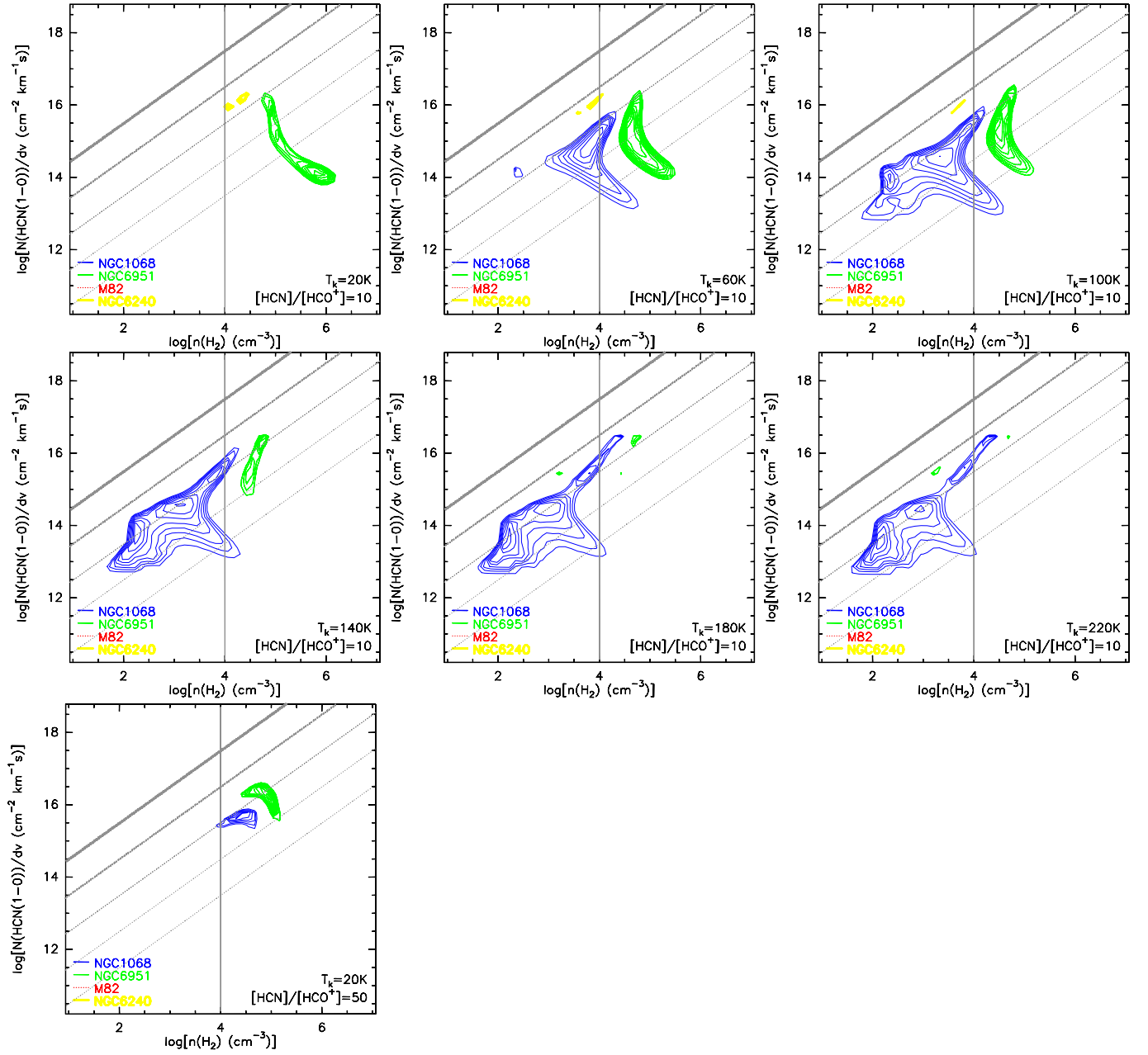


FIG. 7.— Same as Fig. 6 but for abundance ratios of $[\text{HCN}]/[\text{HCO}^+] = 10$ & 50.